KTH ROYAL INSTITUTE
OF TECHNOLOGY

Doctoral Thesis in Chemical Engineering

Gasification of biochars: Evolution of pore structure, effects of alkalis and alkali release

SAIMAN DING

Stockholm, Sweden 2023

Gasification of biochars: Evolution of pore structure, effects of alkalis and alkali release

SAIMAN DING

Academic Dissertation which, with due permission of the KTH Royal Institute of Technology, is submitted for public defence for the Degree of Doctor of Philosophy on Friday the 26th May 2023, at 10:00 a.m. in Kollegiesalen, Brinellvägen 8, Stockholm.

Doctoral Thesis in Chemical Engineering
KTH Royal Institute of Technology
Stockholm, Sweden 2023

ISBN 978-91-8040-545-4
TRITA-CBH-FOU-2023:11

Printed by: Universitetsservice US-AB, Sweden 2023

To my beloved parents: Huaihua Ding & Li Jiang

Your endless love and support have been my steady guide

To my dearest son and husband: Lambert & Jens. F. Isaksson

May it inspire your journey and a reminder of my eternal love for you

Abstract

Renewable energy sources are indispensable to meet the rising demand of energy usage while reducing the negative environmental impact of utilising fossil fuels. Gasification is an efficient technology to convert biogenic waste into valuable gaseous products. The rate of conversion of char, produced in an intermediate step in the conversion, plays an essential role in the conversion of biogenic materials. The conversion of char is significantly affected by properties such as the structure of the char and its alkali content. This thesis presents findings related to the influence of char pore structure development and alkalis content on char gasification, as well as the alkali release during gasification and co-gasification.

Experimental results show that the generation of micropores are directly proportional to the observed reactivity up to 70% of char conversion, after which the catalytic effects of potassium become the dominating factor. Furthermore, investigations of the effect of different intrinsic potassium contents on woody char reactivity demonstrate that no alkali surface saturation point is reached, as is the case for high-ash chars. Application of a modified random pore model enabled a successful capture of the later stages of char conversion in comparison to other kinetic models applied.

Alkali release and sample mass changes were monitored simultaneously, using a thermogravimetric analyser together with a surface ionization detector (TGA-SID). The studies revealed a significant release of alkali as woody char conversion approaches completion during CO_2 gasification. For straw char the release of alkali decreased continuously throughout the conversion process. Similar results were obtained for biochar gasification under steam conditions in a fixed bed reactor. However, in this case the process is more complex, including transfer of alkali between particles inside the fixed bed, which influences char conversion.

Co-gasification of different types of biomass can substantially affect char conversion efficiency. In comparison to pure wood, mixing wood and straw had positive effects on the char conversion for rates below 90% of conversion, while exceeding this degree of conversion resulted in negative effects. The most significant positive effect was observed at a gasification temperature of 900 °C, particularly when using a wood-straw blend of 75 wt%:25 wt%.

The above findings are important for the understanding of the mechanisms of char conversion and are valuable in the design of gasifiers. The research provides with a deeper understanding of char structure development, alkali release, and migration during gasification of biogenic materials.

Keywords: gasification, alkali release, kinetic modelling, char reactivity, pore structure, alkalis effects

Sammanfattning

Förnybara energikällor behövs för att möta den ökande efterfrågan på energianvändning, samtidigt med behoven av att minska den negativa miljöpåverkan som användningen av fossila bränslen medför. Förgasning är en effektiv teknologi för att omvandla biogent avfall till värdefulla gasformiga produkter. I omvandlingsprocessen förkolas biomassan till biokol i ett intermediärt steg. Hastigheten för omvandlingen av biokolet spelar en avgörande roll vid förgasningen av biogena material. Denna omvandling påverkas väsentligt av biokolets egenskaper såsom kolstruktur och dess alkaliinnehåll. I denna avhandling presenteras resultat som relaterar till inverkan av kolstrukturens utveckling och innehåll av alkalier vid förgasningen av biokol samt frigörandet av alkali under förgasning och samförgasning.

Experimentella resultat visar på att genereringen av mikroporer är direkt proportionellt mot observerad reaktivitet upp till 70 procents kolomvandling. Därefter är de katalytiska effekterna huvudsakligen relaterade till kaliumhalten. Vidare så observerades ingen effekt av alkalimättnad av kolytan på biokolets reaktivitet vid studier med biokol från trämaterial med olika halter av kalium, något som observerats tidigare för biokol med högre innehåll av aska. Tillämpning av en modifierad randomiserad modell för utvecklingen av porer resulterade i en lämplig beskrivning av de slutliga stadierna i omvandlingen av biokol jämfört med andra kinetiska modeller.

Frigörandet av alkalier och förändringar i provernas massa undersöktes med hjälp av termogravimetrisk analys tillsammans med en ytjonisationsdetektor (TGA-SID). Studierna visar att en betydande mängd alkalier frigörs mot slutet av biokolets omvandling under koldioxidförgasning. För biokol från halm observerades däremot ett fortsatt minskat frigörande av alkalier under hela omvandlingsprocessen. Liknande resultat erhölls för biokolförgasning under ångförhållanden i en reaktor med en fast bädd. I detta fall är dock processen mer komplex och omfattar även överföring av alkalier mellan partiklar inne i den fasta bädden, vilket påverkar kolomvandlingen.

Samförgasning av olika typer av biomassa kan avsevärt påverka kolomvandlingens verkningsgrad. I jämförelse med rent trä så resulterade en blandning av trä och halm i positiva effekter på kolomvandlingen för omvandlingsgrader under 90 %, medan högre omvandlingsgrader resulterade i negativa effekter. Den mest betydelsefulla positiva effekten observerades vid en förgasningstemperatur på 900°C, särskilt vid en trä-halm-blandning med viktprocentförhållandet 75:25

Resultaten är viktiga för förståelsen av mekanismerna för omvandlingen av kol och är värdefull vid konstruktion av förgasare. Forskningen har gett en djupare

förståelse för utvecklingen av kolstrukturen, frigörande av alkalier och migration under förgasning av biogent material.

Nyckelord: förgasning, frigörande av alkalier, kinetisk modellering, kolreaktivitet, porstruktur, alkalieffekter

List of scientific supplements included in the thesis

Paper I
Effects of porous structure development and ash on the steam gasification reactivity of biochar residues from a commercial gasifier at different temperatures.
Saiman Ding, Efthymios Kantarelis, Klas Engvall
Energies, 13 (2020) 5004.

Paper II
Potassium-induced phenomena and their effects on the intrinsic reactivity of biomass-derived char during steam gasification.
Saiman Ding, Efthymios Kantarelis, Klas Engvall
Submitted to ACS Omega.

Paper III
Real-time monitoring of alkali release during CO_2 gasification of different types of biochar.
Yaxin Ge*, Saiman Ding*, Xiangrui Kong, Efthymios Kantarelis, Klas Engvall, Jan B. C. Pettersson
Fuel, 327 (2022) 125102.

Paper IV
Alkali release behavior during steam gasification of char in a fixed bed reactor and its effect on reactivity.
Saiman Ding*, Yaxin Ge*, Efthymios Kantarelis, Xiangrui Kong, Jan B. C. Pettersson, Klas Engvall
Submitted to Fuel.

Paper V
Online monitoring of alkali release during co-pyrolysis/gasification of forest and agricultural waste: Element migration and synergistic effects.
Yaxin Ge*, Saiman Ding*, Xiangrui Kong, Efthymios Kantarelis, Klas Engvall, Jan B. C. Pettersson
Biomass and bioenergy, 172 (2023) 106745.

*These authors shared primary authorship.

Contribution statement

Paper I: Saiman Ding performed the experiments, analysed the data, and prepared and wrote the original manuscript.

Paper II: Saiman Ding performed the experiments, analysed the data, and prepared and wrote the original manuscript.

Paper III: Saiman Ding equally shared first authorship with Yaxin Ge. Jan Pettersson is the corresponding author. Saiman Ding and Yaxin Ge conducted the experiments, analysed the data, and prepared and wrote the original manuscript.

Paper IV: Saiman Ding equally shared first authorship with Yaxin Ge. Klas Engvall is the corresponding author. Saiman Ding and Yaxin Ge conducted the experiments, analysed the data, and prepared and wrote the original manuscript.

Paper V: Saiman Ding equally shared first authorship with Yaxin Ge. Jan Pettersson is the corresponding author. Saiman Ding and Yaxin Ge conducted the experiments, analysed the data, and prepared and wrote the original manuscript.

List of scientific contributions not included in the thesis

1. Catalytic pyrolysis of lignin using low-cost materials with different acidities and textural properties as catalysts.
Tong Han, Saiman Ding, Weihong Yang, Pär G. Jönsson
Chemical Engineering Journal, 373 (2019) 846–856.

2. Effect of fresh bed materials on alkali release and thermogravimetric behavior during straw gasification.
Yaxin Ge, Saiman Ding, Wennan Zhang, Xiangrui Kong, Klas Engvall, Jan B. C. Pettersson
Fuel (2023) 127143.

3. Effects of used bed materials on char gasification: Investigating the role of element migration using online alkali measurements.
Yaxin Ge, Saiman Ding, Xiangrui Kong, Efthymios Kantarelis, Klas Engvall, Marcus Öhman, Jan B. C. Pettersson
Fuel Processing Technology 238 (2022) 107491.

4. Impacts of fresh bed materials on alkali release and fuel conversion rate during wood pyrolysis and char gasification.
Yaxin Ge, Saiman Ding, Wennan Zhang, Xiangrui Kong, Efthymios Kantarelis, Klas Engvall, Jan B. C. Pettersson
Submitted to Fuel.

5. Alkali release behaviour during CO_2 and steam gasification of different high-pressure produced biochars.
Saiman Ding*, Yaxin Ge*, Efthymios Kantarelis, Xiangrui Kong, Jan B. C. Pettersson, Klas Engvall
Manuscript in preparation.

6. Alkali release and gasification kinetics during gasification of biochar with different alkali contents.
Yaxin Ge*, Saiman Ding*, Xiangrui Kong, Efthymios Kantarelis, Klas Engvall, Jan B. C. Pettersson
Manuscript in preparation.

Contents

Chapter 1

Introduction

Sweden and countries within the European Union have committed to achieving a fossil-free and pollution-free future. Sweden's goal is to have zero net emissions of greenhouse gases into the environment by 2045 [1]. With rising energy demand and concerns about the environmental impact of fossil fuel consumption, biogenic waste feedstocks such as forestry residue and agricultural waste are becoming an attractive resource for renewable energy [2].

Gasification is a feasible technique that can help to facilitate the transition towards a more sustainable and low-carbon energy system by converting biogenic waste materials. This process can be integrated into various industrial processes such as in power generation, chemical manufacturing, steel production, and waste management [3]. It can thus reduce the reliance on fossil fuels and promote the use of renewable energy sources.

Char conversion is an important step in any thermochemical conversion using solid fuel. This step is considered as the rate determining step in an efficient conversion of biogenic solid fuels into a producer gas [4]. An understanding of the mechanisms and kinetics of char gasification is therefore important for gasification reactor design [5] and an overall optimization of gasification based processes.

During gasification, char undergoes structural changes by pore generation, expansion and particle fragmentation [6–8] influencing parameters such as, specific surface area, porosity, and pore size distribution [9–11]. These parameters control active site accessibility for oxidizing agents during char conversion [11,12]. Another important factor influencing the reactivity is the mineral content and composition of the char. Alkali and alkaline earth metals (AAEMs) such as potassium, sodium, calcium, and magnesium act as catalysts and accelerate the char gasification process [13–22]. Due to the complex nature of the overlapping phenomena, it is often difficult to distinguish between different factors affecting biochar reactivity, such as the effects of mineral presence or char structure and temperature history. Consequently, developing well-defined systems that minimize the number of parameters required to analyse biochar gasification remains a challenging task.

Alkali release and migration take place during both char conversion and co-conversion of biomass and are critical phenomena for the interactions between bed materials and char. A surface ionization detector (SID) is an online method for measuring alkali content. The technique is based on selective surface ionization of alkali-containing species and has been developed as an efficient way to characterize dynamic processes involving alkalis. Despite several studies of alkali release during biomass gasification and combustion, there is still much to be learned due to the limited application of analytical tools to monitor alkali metals with sufficient time resolution, as well as the lack of systematic comparisons of different thermal conversion processes. Only a few studies, all focusing on agricultural biochar, have resolved alkali release as a function of char conversion during steam [23,24] and CO_2 [18] gasification. There remains a shortage of comprehensive reports on real-time monitoring of alkali release during char gasification and biomass co-gasification.

Co-gasification is a technology that enables efficient conversion of fuels into syngas and chemicals. It has several advantages over thermal conversion of individual fuels [25]. However, existing studies on fuel co-conversion concentrate mainly on coal-biomass blends [26–28], biomass-only fuel blends receive much less attention. Previous studies on co-gasification have suggested that gasification reactivity can be enhanced by blending biomass with coal, owing to the catalytic influence of AAEM species present in the biomass [29–32].

This dissertation summarizes my work on the combined effects of char structural development and alkalis on char reactivity. Additionally, it provides an improved understanding of alkali release and its relationship to fuel reactivity during char gasification. Studies of co-gasification of different fuels were also conducted. These topics are closely related to issues involving alkalis in various industrial processes, such as catalytic functions, concentrations in syngas, and migration between different materials.

In order to investigate the connection between char reactivity and alkali release during gasification processes, an experimental setup was developed that connects a SID for online alkali measurements to a thermogravimetric analyser (TGA). Using the TGA-SID setup was used to study the release of alkali during the gasification of different chars, as well as the co-gasification of wood and straw. Moreover, a fixed bed reactor combined with SID, diluters, a CO/CO_2 analyser, a scan mobility particle sizer and an optical particle sizer was successfully used to measure alkali. The layout of the dissertation and the research focus at different stages are described below.

1.1 Scope of the thesis

There are three parts to this thesis, as outlined in Figure 1.1:

Stage 1: Understanding pore structure evolution and the effects of alkalis during steam gasification.

In order to gain a comprehensive understanding of the steam gasification process for industrial char, it is necessary to investigate the development of pore structure and the impact of alkalis. Accordingly, Paper I focuses on the evolution of pore structure development throughout the gasification process, and Paper II, examines the effects of potassium-induced phenomena on intrinsic reactivity during steam gasification.

Stage 2: Alkali release behaviour of different biochars during CO_2 and steam gasification.

In Stage 2 of the research, the goal is to advance understanding of alkali mobility and release in diverse biochar gasification processes and to establish the relationship between this behaviour and the char conversion rate under both CO_2 (Paper III) and steam atmosphere (Paper IV).

Stage 3: Alkali migration during co-gasification of wood and straw mixtures.

The goal of Stage 3 is to gain further insight into alkali migration/release and char reactivity during the co-gasification of wood and straw mixtures, as presented in Paper V.

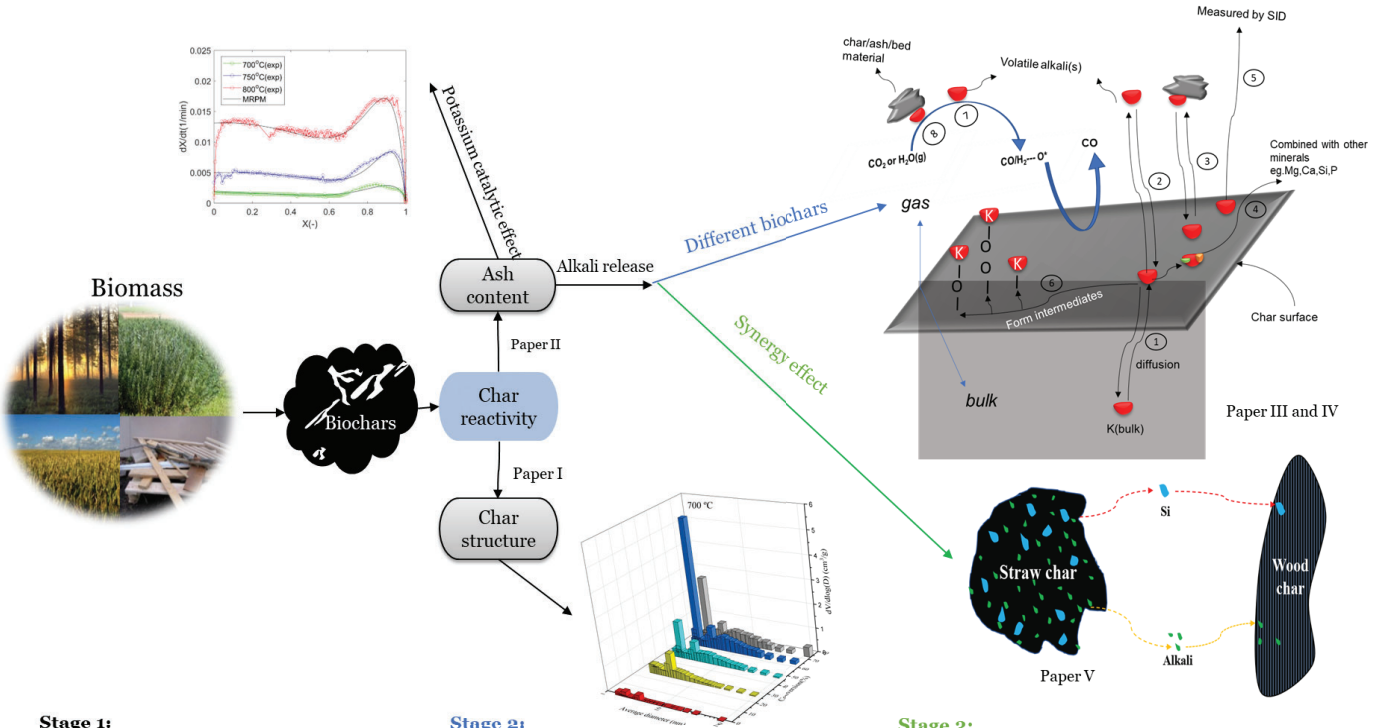

Stage 1:
Understanding of pore structure evolution and alkalis effect on steam gasification
Paper I and Paper II

Stage 2:
Alkali release behaviour of different biochars during CO_2 and steam gasification
Paper III and Paper IV

Stage 3:
Alkali migration during co-gasification of wood-straw mixtures
Paper V

Figure 1.1 The overview of research content.

1.2 Structure of the dissertation

The thesis is divided into seven chapters, each of which focuses on specific aspects of the research conducted during this doctoral study. Chapter 2 presents a general introduction to gasification basics, alkali catalytic behaviour, and various gasification technologies. Chapter 3 presents the experimental setup, materials used, and material characterization. The results of the work reported in Papers I and II, including the pore structure development and the effect of ash on the industrial char during steam gasification, are presented in chapter 4. Research results in papers III and IV are presented in chapter 5, including the alkali release behaviour of different biochars under CO_2 and steam gasification processes. Chapter 6 describes a continuation of the research presented in Paper III and focuses on alkali release and migration during co-gasification of wood and straw in a CO_2 atmosphere. Chapter 7 provides an overview of the general conclusions and recommendations drawn from the thesis.

1.3 Sustainability aspects of the dissertation

All work involved in this dissertation is believed to be beneficial for the development of a sustainable society, where all people can live productive, vibrant and peaceful lives on a healthy planet [33]. The goal of this dissertation is improved understanding of the conversion of biochar such as furniture waste and agricultural biomass in the form of straw. The topic is important for thermochemical conversion processes for added-value products. The work thus falls into the category of sustainable energy production, which is part of the UN Sustainable Development Goal (SDG) 7, which is to seek to ensure access to affordable, reliable, sustainable, and modern energy for all. The use of biogenic waste feedstock also falls into the category of waste management, which is addressed in SDG 11 in regard to sustainable cities and communities [34].

Research to enhance understanding of the conversion of biogenic agricultural waste is an important part of developing processes with higher efficiency and improved fuel flexibility. It can contribute to reducing reliance on non-renewable energy sources and promote a more sustainable future. It is also in line with SDG 13, which aims to take urgent action to combat climate change and its impacts, and with SDG 7 as regards providing affordable and clean energy.

Chapter 2

Background

This chapter provides general information on gasification basics, alkali catalytic behaviour and gasification technologies.

2.1 Gasification

The negative environmental impact of fossil fuels and the growing demand for energy have contributed to increasing recognition that biogenic waste feedstocks are an attractive resource for producing chemicals and fuels from non-fossil sources [2]. Gasification is a feasible technique for primary conversion of these feedstocks into an intermediate gaseous feedstock that can be further upgraded into useful end user products such as chemicals, heat, and power [3]. The biomass conversion process includes drying, pyrolysis, gasification, and partial combustion of the residual char, as well as homogeneous gas phase reactions. The gasification of char involves a set of heterogeneous reactions with different gasifying agents, such as CO_2, H_2O, O_2, and mixtures thereof, and is generally the rate-determining step [4]. Designing efficient gasification reactors thus requires a clear understanding of the char gasification mechanism and kinetics.

Two important factors that can influence the char gasification process are the char pore structure and the presence of alkali and alkaline earth metals (AAEM) [35]. AAEMs such as potassium, sodium, calcium, and magnesium act as catalysts, speeding up the char gasification process and promoting heterogeneous reactions between the char and gasifying agents [13–22]. The primary focus of this work is thus the experimental investigation of char gasification and the effect of alkalis.

The following review of phenomena related to biomass gasification is intended to facilitate discussion of the results.

2.1.1 Gasification fundamentals

The biomass gasification process uses high temperatures and various gasifying agents to efficiently convert a solid organic compound into gas vapour and a solid phase [36]. The resultant gas is known as ‘producer gas’ and can be further upgraded into ‘syngas’ for use in power generation or biofuels production. The solid phase consists mainly of unconverted carbon and a small fraction of ash present in the

treated biomass [37]. The biomass conversion process involves the partial oxidation of the carbon in raw materials in the presence of various gasifying agents. Figure 2.1 shows a simplified general reaction path of different gasification steps.

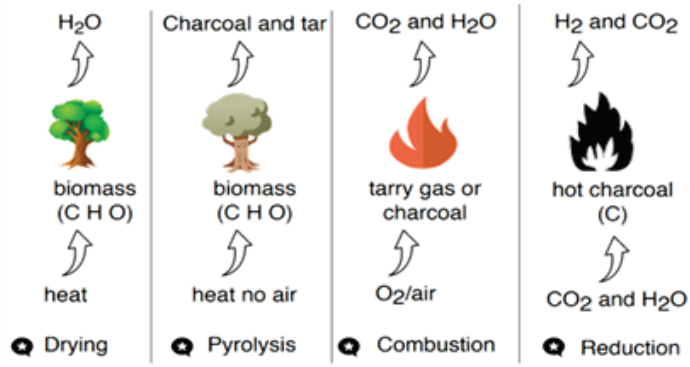

Figure 2.1 A simplified schematic representation of the gasification.

The main steps of the gasification process are:

Drying (endothermic stage)

The moisture content in biomass varies [38] and is removed during the drying stage. The heat required in this stage is proportional to the moisture content of the feedstock. A high moisture content causes energy loss and adversely affects the quality of the gas product [39].

$$\text{Biomass(wet)} \rightarrow \text{Biomass(dry)} + H_2O\text{(steam)} \qquad 2\text{-}1$$

Pyrolysis (endothermic stage)

During pyrolysis, rapid heating converts biomass into gases (e.g., H_2, CO, CO_2, CH_4, and other small hydrocarbons), liquids (tar and water), and solids (char).

The pyrolysis reactions occur in a temperature range between 150 and 700 °C, forming different products depending on the temperature [38]. Hemicellulose starts decomposing within 150 °C to 350 °C, while the cellulose present in biomass decomposes at 275 °C to 350 °C. The lignin part gets is converted into aromatics with a temperature range of 250 °C to 500 °C. At this stage, the reactions are endothermic and the heat needed is provided by the combustion stage of the process. The pyrolysis process can be schematized with the following overall reaction [40]:

$$\text{Biomass} \rightarrow H_2 + CO + CO_2 + CH_4 + H_2O(g) + \text{Tar} + \text{Char} \qquad 2\text{-}2$$

The term 'tar' typically refers to the condensable fraction of organic compounds produced during gasification. These condensable hydrocarbons can range in molecular weight from 78 (benzene) to 300 or more [41,42]. They are usually divided into two categories: water-soluble (phenolic) compounds and non-water-soluble (aromatic) compounds [41,42]. Tar maturation depends on temperature [41,43]. Primary tars (mixed oxygenates) are formed at lower temperatures (400 °C). As the temperature increases from 500 °C to 700 °C, tar is transformed into secondary tars, including phenolic ethers, alkyl phenolics, and heterocyclic ethers. When the temperature exceeds 800 °C, tertiary tars (PAH) are formed. Excessive tar content in the fuel gas reduces the overall efficiency of biomass and increases the overall separating cost of the plant [44,45] as it can clog filters and even polymerize into complex molecules [46].

Combustion (exothermic stage)

Combustion of the biomass is necessary to obtain the thermal energy needed for the endothermic processes and to maintain the operating temperature at its required value. The amount of gasifying agent is usually controlled to avoid reaching the ash slagging temperature [47]. The main reactions taking place during the oxidation phase are char combustion (2-3), partial oxidation (2-4),and hydrogen combustion (2-5).

$$C + O_2 \rightarrow CO_2 \quad \text{2-3}$$
$$C + O_2 \rightarrow 2CO \quad \text{2-4}$$
$$H_2 + \frac{1}{2}O_2 \rightarrow H_2O \quad \text{2-5}$$

Reduction (endothermic stage)

The reduction stage contains reactions between gases and a solid-gas reaction. In this stage, tar, carbon, carbon dioxide, hydrogen, and water vapour are reduced, resulting in the formation of combustible gases. The main reactions (2-6 to 2-9) that occur during the reduction step include tar reforming, Boudouard reaction, char reforming, water-gas reaction and methanation. Reactions 2-7 and 2-8 are commonly referred to as the gasification reactions:

$$C_xH_y + H_2O \rightarrow xCO + (x + y/2)H_2 \quad \text{2-6}$$
$$C + CO_2 \leftrightarrow 2CO \quad \text{2-7}$$
$$C + H_2O \leftrightarrow CO + H_2 \quad \text{2-8}$$
$$CO + H_2 \leftrightarrow CH_4 + H_2O \quad \text{2-9}$$

2.1.2 Gasification parameters

Char reactivity depends primarily on the properties of the biomass feedstocks and the operating conditions, which further determine the subsequent gasification rate of the char [35]. In the gasifier, the temperature will influence the yield of char and

its properties and further char gasification. The heating rate normally has a greater effect on the char reactivity in the early pyrolysis stage, a negligible effect when reaching the final temperature in the later gasification stage. This section summarizes the effect of different gasification parameters on biomass gasification from the point of char generation and gasification under various operating conditions [48].

Biomass type

Biomass is a broad term that encompasses such things as agricultural, forestry and municipal waste, energy crops, and woody biomass [49,50]. Biomass is mostly composed of cellulose, hemicellulose, and lignin. Di Blasi et al. [51] analysed the chemical composition of wood chips and some agricultural residues. They found that the hemicellulose and cellulose together make up about 35–60%, while the lignin is 15–30%. The remainder is ash and extractives. Lv et al. [52] compared the effect of cellulose and lignin on biomass gasification with six types of biomasses whose cellulose content varied from 55% to 85% and lignin content from 10% to 35%. The tar and gas yields depended on the cellulose content and increased with increasing cellulose in the biomass.

Moisture content also plays a significant role when dealing with biomass. Low moisture content biomass (<15 wt%) is suitable for gasifiers. Energy requirements increase as the moisture content increases [53]. Basu et al. [45] compared analysed the moisture content of various biomass feedstocks and concluded that wheat straw, rice husk are considered the better feedstocks due to their low moisture content.

The presence of inorganic materials such as alkali and alkaline earth metals (AAEM) can also affect the composition and reactivity of the biomass. While these inorganic materials may constitute only a small percentage of the biomass, they play a critical role in homogeneous and heterogeneous reactions during pyrolysis and gasification, which in turn affect the properties of the final products, including chars [36]. The role of AAEM is further discussed in section 2.2.

Temperature and heating rate

Temperature is the most critical operating parameter throughout the entire biomass gasification process, surpassing all other factors (heating rate, pressure, and residence time). The temperature has a significant effect not only on the char production via drying and pyrolysis, but also on the performance of the char gasification. Increased process temperature results in a drop in the H/C and O/C ratios, which leads to an increase in the carbonization degree of biochar. Meanwhile, due to its low polarity and strong hydrophobicity, biochar with an exceptionally low O/C ratio may boost its potential to collect CO_2 in the presence of water [54,55]. While the heating rate in the gasifier is critical during the initial stage of biomass pyrolysis, once the final gasification temperature is reached, the heating rate has

only a minor effect on the char gasification. Biomass pyrolysis can be divided into slow, fast, or rapid pyrolysis based on the heating rate, which generally affects the char yield as well as its properties and reactivity [56,57]. Furthermore, the temperature of char particle generation history influences its reactivity [58]. For example, Septien et al. [59] concluded that increasing pyrolysis heating rates from 1°C/s to 1000°C/s results in a more reactive char with higher gasification rates. The higher char reactivity at high heating rates may be attributed to a change in the char's morphology [6–8] or its textural properties due to the formation of a larger pore volume. The pore volume comprises mainly mesopores and macropores, as opposed to a lower pore volume of mainly micropores at low heating rates [7]. Textural properties of biomass char are also significantly changed during the gasification process, expressed as an evident increase in porosity and surface area [23,60–66].

Gasifying agents

The primary reagents for biomass gasification are steam, air, and oxygen, or combinations of these. The composition of the resultant gas products is highly dependent on the gasification agent used, which also has a substantial effect on the gas–solid interaction behaviours during char gasification. While air and oxygen are typically employed as oxidizing mediums that combine with carbon to generate exothermic heat for the reaction, steam is frequently added to form hydrogen-rich syngas products. Carbon dioxide produced during pyrolysis or gasification, as well as steam generated during the drying of raw biomass, will also act as gasifying reagents in a gasifier.

Char reaction with CO_2 can optimize the operating conditions inside the reactor, minimize the residual char, and improve the quality of gas products. Steam char gasification can produce hydrogen-rich gas products, or syngas, which is an intermediate energy carrier for chemical industries. Compared to char–O_2 reactions, carbon reaction with steam or CO_2 is slower. Char–steam generally has a much higher reaction rate than char–CO_2 gasification [36].

2.2 The role of AAEM on biomass gasification

AAEMs are of particular importance in relation to the effects of inorganic content on biomass gasification [35,64,67–71]. In case of biomass-based feedstocks, potassium (K) is of greatest importance among the inherent AAEM species [64,67], followed by calcium (Ca), which is abundant in woody chars, typically as carbonate or oxide [72–76]. AAEMs can be divided into two categories: inherent and loaded. Inherent AAEM are naturally present in biomass feedstock. They can have a significant impact on the physical and chemical properties of the biomass, as well as on its reactivity during the gasification process. By contrast, loaded AAEMs are

deliberately added to the biomass feedstock as catalysts or other additives to enhance the performance and efficiency of the gasification process. The effect of AAEMs on gasification is discussed in terms of gas product distribution and gasification reactivity.

2.2.1 Effect of inherent AAEMs

The inorganic species in biomass can be classified into four categories: water-soluble, ion-exchangeable, acid-soluble, and residual [77,78]. Of the AAEMs, potassium (K) is the most active element with catalytic properties [64,67]. Other elements that affect catalytic gasification reactivity include Na and Mg [20,22], which are generally less abundant in biomass than K. Several researchers report that the presence of Ca can inhibit potassium deactivation [79–82], and possibly boost catalytic impact by forming calcium and potassium bimetallic active compounds [80,83]. The temperature of the ashing analysis is vital to measuring the content of inherent AAEMs accurately. Currently, the temperature in the widely used high temperature ashing treatment can be as high as 500–815 °C. At those temperatures, volatile minerals such as K and Na are partially volatilized and the form of minerals in biomass is destroyed [84].

Guo et al. [85] have shown that inherent AAEMs have a significant effect on product distribution in corn O_2 gasification, and that the effect is closely related to gasification temperature. They showed that inherent AAEMs were favourable for CH_4 and C_xH_y production at 600–800 °C. Above 750 °C, AAEMs promoted H_2 and CO generation as well as tar reduction, indicating that the inherent AAEMs showed higher catalytic activity at higher temperatures. When the temperature rose to 950 °C, the volatilization of alkalis had a negative effect on tar steam reforming compared to 850 °C [86]. Heung-Min Yoo et al. [87] tested air gasification characteristics of fruit bunches with raw, water leached and nitric acid leached samples in bubbling fluidized bed reactor at 900 °C. The yield of H_2 and CO in leached fruit bunches both increased compared to the raw sample. This may be due to the reduction of agglomeration with the removal of AAEM compounds caused by the washing pre-treatment.

The different AAEM species in woody biomass and straw can lead to different product distributions during the steam gasification process. For example, in straw steam gasification, the presence of AAEMs enhanced the production of H_2 and CO_2, while inhibiting the production of CO, CH_4, C_2H_4 and C_2H_6 at 900 °C. However, in woody biochar steam gasification, the inherent AAEMs have an insignificant catalytic effect on the water–gas shift reaction, although AAEMs significantly catalysed the biochar gasification [70].

Besides product distribution, AAEMs can affect the gasification reactivity of biomass char which is another important factor in biomass gasification. Zhang et al.

[88] found that inherent alkali metals were more effective than inherent calcium during pressurized steam gasification. Potassium played the most important catalytic role among the native AAEM species, and its overall activity reached a maximum during gasification, indicating the presence of optimal clusters or particle sizes of K catalyst [64]. A steam gasification experiment with biochar by Yip et al. [70] indicated that Na, K, and Ca retained in the biochar were the key catalytic species, with the catalytic effect appearing to be in the order K > Na > Ca. Coal gasification by Du et al. [89] showed different results: Ca had more significant effects on char structure and devolatilization behaviour than Na, probably because coal gasification took place at higher temperatures. In addition to AAEMs, other factors such as micropore structure and internal surface area, active sites and low silicon content of the biomass have been found to play a major role in determining the gasification reactivity of biomass char [90]. When the char contains high levels of silicon, alkali silicates are formed at low temperatures, which limits their catalytic activity.

2.2.2 Effect of loaded AAEMs

The loaded AAEMs in char has different catalytic effects [17]. The catalytic effect of Ca is slightly higher than that of the alkali metals (K, Na) during catalytic coal gasification [91]. Along with the formation of activation centres on the char surface, the CO_2 gasification reactivity of fir char increased in the order K > Na > Ca > Mg. The crystal structure of the char was improved by Na and Ca, while the degree of graphitization order of the carbon structure can be enhanced by Mg. However, AAEM nitrates exhibited different catalytic properties: Na-char > Ca-char > K-char >Mg-char > raw char [92]. The 5 wt% Na loaded char had the highest reactivity among the selected catalysts and loadings. The AAEM catalyst effect was influenced not only by the gasification temperature and agent but also by the composition of the biomass. Eutectic mixtures of alkali metal halides, carbonates, and sulphates in binary and ternary forms are more efficient for char gasification using CO_2 and steam than individual salts. This is due to the lower melting point of eutectics, which facilitates greater contact between the catalyst and carbon matrix [93].

Research on the use of AAEM as a catalyst in biomass gasification has shown that different additions have varying effects on the product gas distribution. For instance, adding CaO can both speed up the gasification reaction and increase H_2 production, as well as decrease the production of CO and CO_2 [94]. Similar results were observed in coal gasification, where Ca additives were found to be effective in increasing H_2 production [95]. An optimal loading was found to be less than 1 wt% [96]. Studies on catalytic steam gasification [97] also highlighted the positive effects of CaO and coal bottom ash, particularly Mg and Ca, on H_2 yield. However, increasing the concentration of Na to 5 wt% led to a peak in CO release rate, which decreased as the catalyst loading continued to increase [92].

The presence of metal particles deposited on the char surface can block active sites and decrease H_2 production during biochar gasification. Alkalis additives, such as NaOH, KOH, and $Ca(OH)_2$, can improve H_2 production by facilitating the water-gas shift reaction, which forms formate salts, and also decrease the formation of tar and char. Additionally, CO_2 is the primary gaseous product when metallic carbonates and bicarbonates (K_2CO_3, Na_2CO_3, and $NaHCO_3$) are present. It is, however important to note that catalytic performance can be influenced by various metal ions and their concentrations [98]. Incorporating AAEM into the biomass can enhance the carbon content in the resulting gaseous products, resulting in improved product quality. Furthermore, loading the biomass with alkali metals can aid in breaking down polycyclic aromatic hydrocarbons (PAHs) into 1–2 aromatic rings light tar.

2.3 Mechanism of AAEM catalytic char gasification

Chen et al. proposed a mechanism of catalytic gasification of carbon, using AAEM catalysts in the presence of CO_2 and H_2O [99]. They found that catalytic gasification was based on the alkali–C interaction by affecting the electron cloud density and strength and energy of the C–C bond (Figure 2.2). The affinity between the bridge C atom and the O atom is strongly affected by the local electron density of the bridge C atom. By attaching an alkali atom to the edge, the net charge of the bridge atom is substantially increased because of the conjugate effect. Since H_2O and CO_2 prefer to chemisorb on atoms with larger electron densities, the presence of alkali metal will facilitate the chemisorption of H_2O and CO_2 on the bridge C atom, and as a result, the C-O-M (where M refers to AAEM) group shows the catalytic activity.

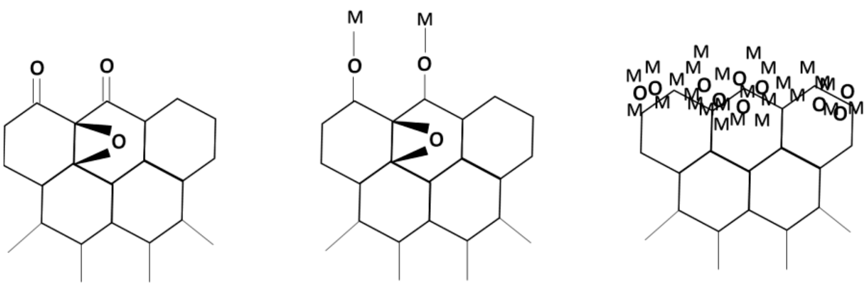

Figure 2.2 Different states of oxygen complexes in uncatalysed and alkali-catalysed systems (adapted from Chen et al. [99]).

Another theory, proposed by McKee [100,101], suggests that the catalytic effect of alkali carbonate occurs through a redox cycle that dissociates CO_2/H_2O into CO/H_2 and transfers atomic oxygen into the char (Figure 2.3). In a CO_2 atmosphere, carbonate decomposes into metal oxides and metals. For steam gasification, the catalytic intermediates of carbonate were metallic hydroxides and metals. The influence of AAEM on steam char conversion has been described as an oxygen

transfer mechanism via the metal M, involving the reaction of salts with carbon, followed by subsequent metal oxidation by the gaseous environment [100–102]. As a result, the enhanced oxygen exchange between the gasifying atmosphere and the reacting solid increases the carbon conversion rate, leading to higher reactivity and gas production.

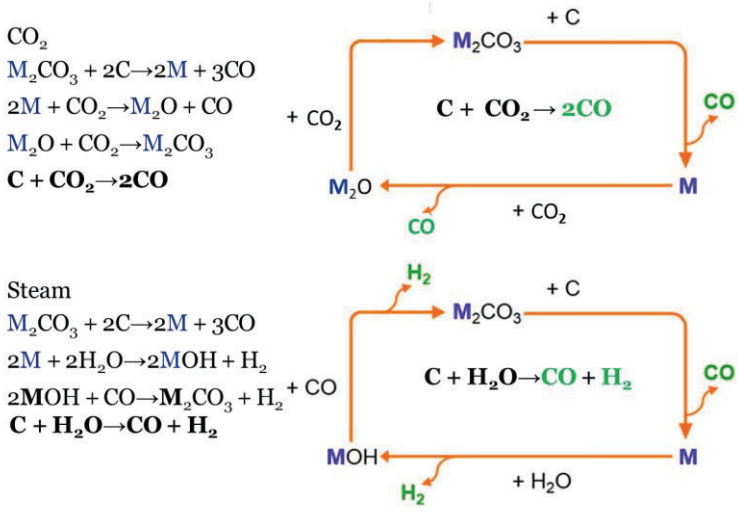

Figure 2.3 Reaction mechanism for CO_2 and H_2O gasification based on redox cycle. Based on references [100–102].

The interaction between AAEMs and biochar under CO_2 conditions is different from the reaction under steam conditions [103]. Feng et al. state that CO_2 is too large to reach the interior of the biochar and thus has little impact on its aromatic structures beyond the gas-solid interface. As a result, only the AAEM species on the surface of the biochar have catalytic characteristics and the transformation from small to large aromatic rings is slower. By contrast, steam is adsorbed and dissociated into H and OH radicals, allowing the reaction to occur throughout the entire biochar particle. During the migration of AAEM species, continuous bond breaking and reforming leads to further condensation of aromatic rings.

The presence of K has a more significant impact on the H_2O/CO_2 gasification of biochar than the presence of Ca species. The different gasification rates are due to differences in the migration characteristics and mechanisms of oxygen transformation and intermediate hybridization [69,104]. During the thermal conversion of biochar, AAEM species are released and provide more active sites for catalytic reactions, and K is reduced to -COK and/or -CK structures to form active sites on the biochar surface. Ca participates in the gasification reaction by forming -COCa and -COOCa functional groups with more stable divalent bonds, leading to a

lower gasification rate. The catalytic mechanism of K mainly affects the formation of oxygen-containing functional groups and the transformation of small ring molecules into larger rings, while the catalytic effect of Ca increases the proportion of large aromatic ring structures [103].

Mei et al. have proposed that the catalytic effect of alkali on gasification rate may result from the alkali–gas interaction [105]. The gasification CO_2 can be activated on the alkali surface, resulting in a higher activity of O*, which can easily attack the carbon matrix at a high temperature, thus speeding up the reaction with the carbon matrix, as schematically described in Figure 2.4.

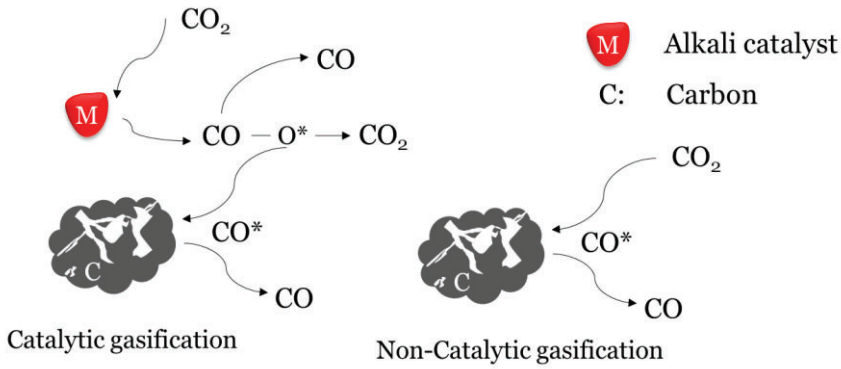

Figure 2.4 Schematics of the mechanism for the C-alkali interaction during CO_2 gasification. Adapted from reference [105].

2.4 Gasifier technologies

The size and type of gasifier selected for a specific process depend on several parameters, including the product demands, moisture content, and fuel availability. As shown in Figure 2.5, the main types of reactors used in the biomass gasification process are fixed bed (a and b), fluidized bed (c and d), and entrained flow (e).

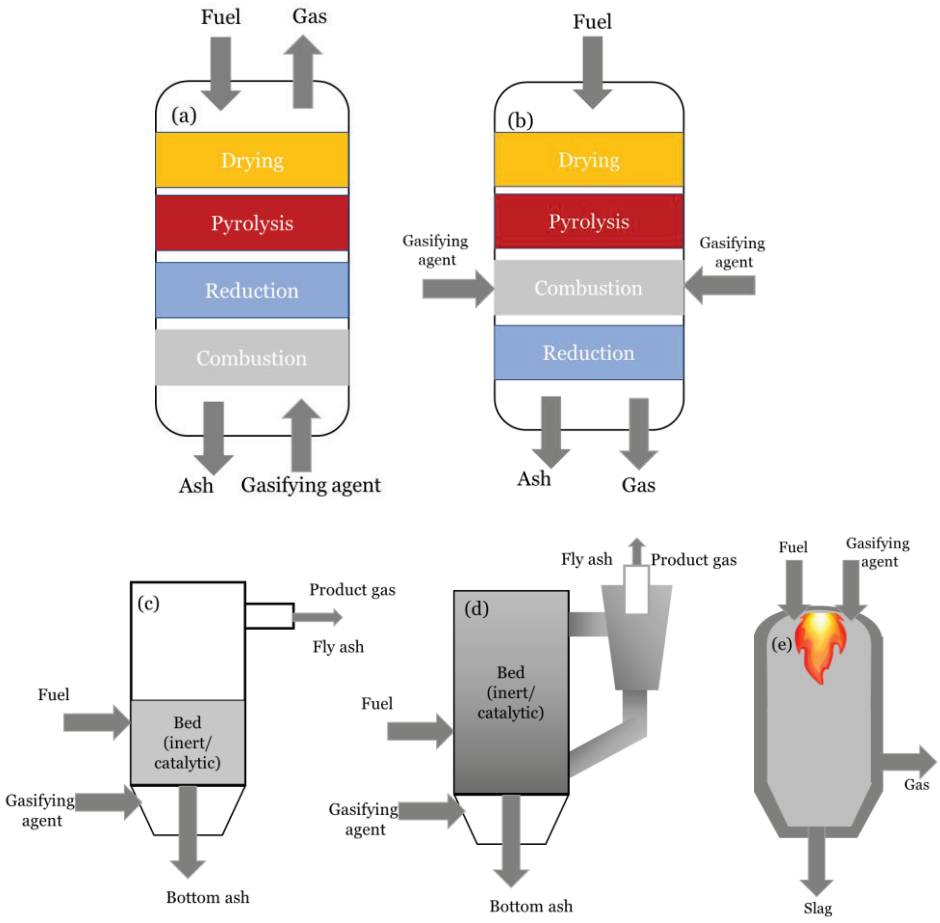

Figure 2.5: Types of gasifiers [45,106]: (a) fixed bed updraft gasifier, (b) fixed bed downdraft gasifier, (c) bubbling fluidized bed gasifier, (d) circulating fluidized bed gasifier, (e) entrained flow gasifier.

Fixed bed gasifier

Fixed or moving bed gasifiers [36] can be classified into updraft and downdraft (Figure 2.5a and 2.5b). They are ideally used for small-scale biomass processes with a capacity <10 $MW_{thermal}$ [45]. In the updraft configuration, the solid moves downwards and the gas produced flows upwards. The size, shape, and moisture content of the fuel are not critical, and even fuels with high water content can be gasified. However, the product gas quality is generally low with a high tar content (5-20%) [107]. In the downdraft configuration, both the solid and the gas move downwards. This configuration is typically used for gasifying woody biomass with uniform sizes and shapes. Producer gas from a downdraft gasifier has lower tar

levels (<1%), a higher temperature, and less particulate matter than gas from an updraft gasifier.

Fluidized bed gasifier

Fluidized bed gasifiers operate on the principle of fluidization, where a gas stream is passed through a bed of particles that behave like a fluid. The two most common types of fluidized bed reactors are the bubbling fluidized bed (BFB) and the circulating fluidized bed (CFB) [53,108]. In a BFB (Figure 2.5c), the gasifying agent is supplied from the bottom through the bed with a velocity between 1 and 3 m/s. A BFB normally operates at a temperature range between 650 °C and 950 °C at pressures of 1-35 bar on a relatively large scale (>10 $MW_{thermal}$). It can handle heterogeneous fuels with particle sizes up to a few centimetres.

In a CFB (Figure 2.5d), the gasification process is divided into two stages. The first stage is a bubbling fluidized bed where combustion reactions generate heat, and the second stage is a high-speed gas (5–10 m/s) to allow the dragging of the solid, where pyrolysis and gasification take place. It typically operates at temperatures of 800-1000 °C, below the ash melting temperature to prevent agglomeration of sticky ash particles. A CFB is well-suited to fuel particles with high ash content. It results in higher quality product gas and higher throughput than a BFB. It is important to note that defluidization may occur from particle agglomeration, especially when agricultural crops and waste are used as feedstock in the gasification process. This is because the ash from agricultural crops and waste has a higher alkali content (e.g. sodium and potassium), which can form low-melting eutectics with silica in the sand, that is, commonly used as a bed material in FBG processes.

Entrained flow gasifier

An entrained flow reactor (Figure 2.5e) normally operates at a very high temperature (>1200–1500 °C) at pressures of 20–70 bar on a relatively large scale. Although the high reaction activity of biomass allows biomass gasification to be carried out at a relatively lower temperature range of 700–1050 °C, this is not a popular option because of the low ash melting points of biomass and the difficulties of bulk collection. Furthermore, the ash melting point can be a critical factor to consider when choosing the design and operating temperatures of biomass gasifiers [109].

Comparison of gasification technologies

Fixed bed gasifiers are simple and easy to operate, but they have limited scalability due to poor mixing and heat transfer, resulting in uneven fuel and temperature distribution within the gasifier. Therefore, it is difficult to scale-up this type of gasifier. Downdraft reactors are designed to handle only dense and solid feedstock with minimal water content to ensure efficient gas flow and prevent operational difficulties. The updraft gasifier, on the other hand, has a high tar production rate,

making it unsuitable for producing clean product gas, but suitable for gasifying low-volatility feedstocks like charcoal [45].

The FBG gasifier, particularly the CFB type, is widely recognized as the most efficient type of gasifier. It is capable of effectively processing fuels with high levels of volatiles and has a high fuel capacity. The FBG gasifier is robust in accommodating variations in fuel composition. Additionally, it ensures excellent particle/gas contact and fuel/bed heat transfer [110]. However, the operation of a FBG is quite complex, requiring simultaneous control of the air supply, bed material, and feedstock. The product gas may contain high levels of particulates, which can circulate and erode equipment. The high-pressure conditions can also result in low volumetric gas flow rates and other operational complications such as particle agglomeration and defluidization, particularly when high ash content biomass is used.

The EFG has many benefits, including being easy to scale-up. It offers high fuel flexibility, a uniform temperature, and high carbon conversion with low tar concentration [111]. However, pre-treatment of the feedstock is necessary to lower its bulk density and moisture content. The high temperature results in medium thermal efficiency due to increased energy losses.

Chapter 3

Materials and methods

3.1 Raw material

3.1.1 Biomass

Four different types of biomass were investigated: pine, a mixture of wood and branches, furniture waste, and straw. Table 3.1 displays the results of proximate, ultimate, and inductively coupled plasma optical emission spectroscopy (ICP-OES) analyses for mineral matter conducted on the biomass materials used. The biomasses were used to explore alkali release during biomass/char CO_2 gasification in Paper IV. Additionally, pine and straw were used in a co-gasification study in Paper V.

3.1.2 Biochars

The biochar (OC) used in Papers I and II is unreacted char collected from an entrained flow gasifier, using pine wood as feedstock with a maximum particle diameter of 0.1 mm. OC was collected from the scrubber sedimentation tank and placed downstream of the gasifier. The biomass was gasified at a temperature around 1200 °C using air as a gasification agent at an equivalence ratio of 0.28–0.32. Leached char samples (2LC and 48LC) were prepared using deionized water as a leaching agent.

The biochars investigated in Paper IV were produced from those mentioned in 3.1.1. Biochar IC was gathered from the same gasifier as OC, but from a different batch. Straw char (ST) was derived from straw char pellets, while furniture waste char was produced using furniture waste (FW) supplied by IKEA Co. To produce straw char and furniture waste char, the biomasses was pyrolysed in a fixed-bed reactor with N_2 gas at a temperature of 950 °C for two hours to remove volatile matter. The proximate and elemental analyses of all types of biochars are listed in Table 3.2.

Table 3.1 Proximate, ultimate, and ICP-OES analysis of the biomasses.

Sample	Pine	Wood and branches	Furniture waste	Straw
Ultimate analysis (wt%, dry basis)				
C	50.9	47.3	48.7	42.9
H	6.2	6.47	6.1	5.86
N	0.1	0.06	4.08	0.48
O*	42.8	46.2	41.1	50.8
S	0.01	0	0.04	1.62
Cl	< 0.02	-[a]	0.016	-[a]
Proximate analysis (wt%, delivered basis)				
Moisture	7.2	6.4	5.6	0.2
Volatile	83.6	79.3	76.2	74.4
Ash	0.3	0.3	0.5	6.2
Fixed Carbon	8.9	13.9	17.7	19.2
		Mineral matter (mg/kg)		
K	340	1430	530	7790
Na	110	30	130	130
Ca	560	1200	1150	2000
Si	40	20	100	6160
P	40	70	10	260
Al	80	20	30	80
Fe	50	10	20	70
Mg	110	150	110	520
Mn	70	50	90	20
Zn	10	10	10	10

[a]Samples not analysed for Cl. *Calculated from difference: O%=100%-C%-H%-N%-S%.

Table 3.2 Ultimate, proximate , and ICP-OES analysis of biochars.

	Papers I and II				Paper IV	
Samples	OC	2LC	48LC	IC	ST char	FW char
Ultimate analysis (wt%, dry basis)						
C	85.77	87.28	87.92	82.5	69.5	81.7
H	1.12	0.95	0.88	1.02	1.3	1.3
N	0.37	0.36	0.36	0.25	0.5	3.1
O*	5.76	6.04	7.38	16.2	28.5	13.9
S	0.09	0.07	0.06	0.03	0.2	-
Proximate analysis (wt%, delivered basis)						
Moisture	0.6	0.24	0	0	0.2	0
Volatile	4.53	3.98	3.51	9.7	9.38	9.09
Ash	6.9	5.3	3.4	4.58	18.79	2.03
Fixed Carbon	88.57	90.72	93.09	85.72	71.6	88.8
Mineral matter (mg/kg)						
K	5690	3060	766	2500	28000	3330
Na	755	495	173	230	506	767
Ca	11200	10200	9320	16900	8330	3820
Si	1450	1920	846	950	39800	1300
P	677	701	693	230	1170	229
Al	336	340	330	460	457	158
Fe	720	616	599	620	386	214
Mg	2660	2600	2350	3120	2060	705
Mn	1540	1550	1530	1810	84.9	420

* Calculated from difference: O%=100%-C%-H%-N%-S%.

3.2 Experimental methods

3.2.1 TGA

The steam gasification of biochar in Papers I and II was performed using a NETZCSH ST490 F3 thermogravimetric analyser (TGA). Thermogravimetry is a technique for determining the rate of chemical reactions based on the change in the weight of a sample caused by the reaction. The primary advantage of TGA is that it

can easily obtain time-resolved data and enables accurate kinetics characterization by assessing the reaction rate as a function of char conversion (X).

3.2.2 TGA-SID system

CO_2 gasification of biochars and co-gasification of straw and pine was conducted in a TGA-SID system in Papers III and V. A schematic view of the TGA-SID system is shown in Figure 3.1. The setup consisted of the TGA and a SID for continuous alkali measurements in the outlet flow from the TGA. The SID measures the total concentration of alkalis in the flow from the TGA. The main component of the SID is a hot Pt filament (1500 K) where alkali containing molecules and aerosol particles decompose and produce alkali ions by surface ionization. The surface ionization process is highly sensitive and selective for elements with low ionization potentials like K and Na, while contributions from other elements are negligible and can be ignored. The ions emitted from the Pt filament subsequently diffuse to a nearby collector and give rise to a current that is monitored during the experiments [112–114]. The SID signal was transformed into an alkali concentration based on separate laboratory experiments, using KCl aerosol particles with a known concentration. During the experiments, the SID was operated with a total working flow of 700 ml min^{-1}, including the outlet gas from the TGA and an additional N_2 dilution gas. A detailed description of the reaction process is given in Papers III and V.

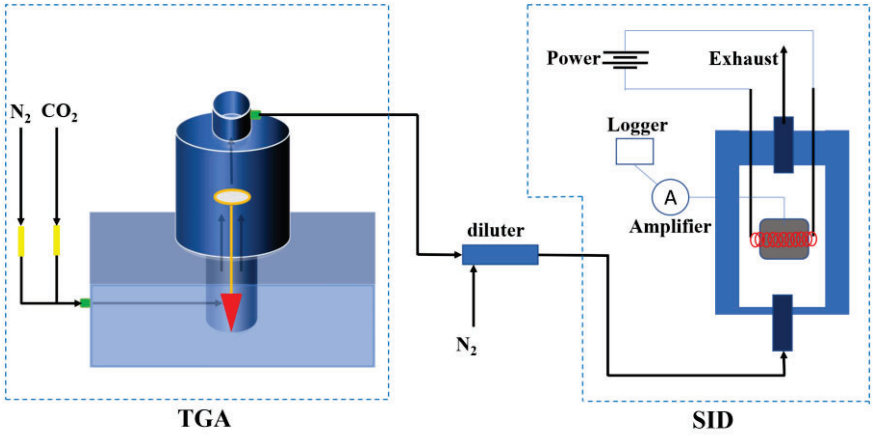

Figure 3.1 Schematic view of the TGA-SID system.

3.2.3 Fixed bed reactor

Alkali release during steam gasification (Paper IV) was performed in a laboratory batch-scale fixed bed reactor. The experimental rig (Figure 3.2) consisted of three sections: the inlet line, the reactor and the exit line. The inlet line contained a nitrogen mass flow controller (labelled MFC in the figure) and a water vapour

saturator. The furnace was stainless steel, with the main reaction chamber 400 mm in height and 17 mm inner diameter. The samples were located at the top of the reactor and heated up to temperatures ranging from 800 °C–950 °C. The char samples were placed on a plate with a 20μm aperture that was supported by another stainless tube with a 14 mm diameter and 300 mm long. A thermocouple was placed close to the char bed to monitor the temperature. Steam with a concentration of 8.2 vol% was provided by a water vapour saturator at 42 °C. Two heating tapes were installed at the inlet tube (150 °C) and outlet tube (200 °C) of the reactor to prevent steam condensation. The flue gas (exit line) was first diluted with an additional 5 Nl/min N_2 and then divided into two streams. One was connected to the exhaust, and the other to the manifold, which led to different analytical instruments: a CO/CO_2 analyser (model NGA 2000, Emerson, labelled GRIMM in the figure), a SID, and a scan mobility particle sizer (SMPS; model 3936, TSI Inc.) See Paper III for more detailed information.

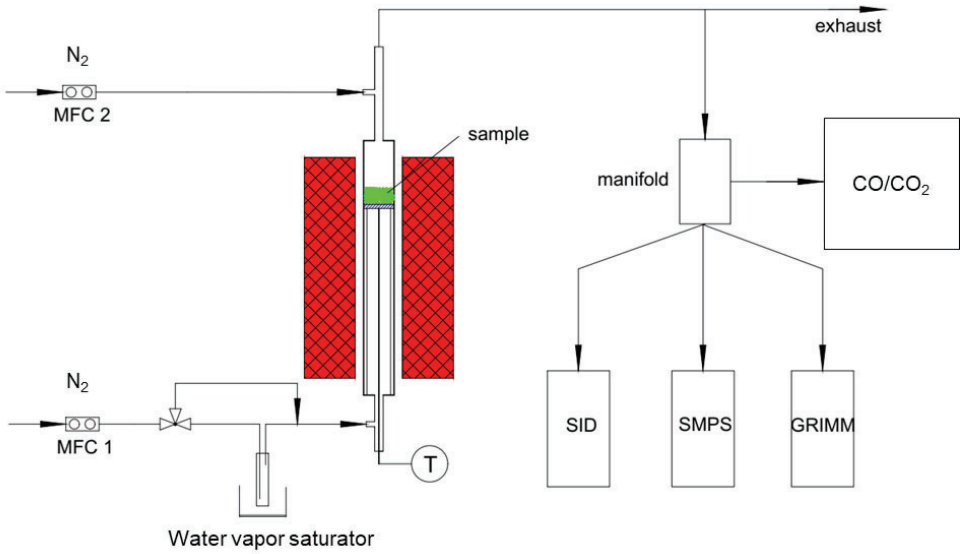

Figure 3.2 Schematic view of laboratory scale reactor system.

3.2.4 Solids characterization technique

The biochar was characterized as follows:

The texture properties of biochar were determined by N_2 adsorption (Micromeritics ASAP 2000) based on the BET (Brunauer - Emmett - Teller) method [115,116]. Prior to analysis, each sample was degassed at 250 °C overnight. The pore size

distribution was determined using the BJH (Barrett-Joyner-Halenda) method, while the micropore volume was determined using the t-plot method.

Scanning electron microscopy with energy dispersive spectroscopy (SEM-EDS) was employed to analyse the relative content of elements, including K, Na, Al, Mg, Ca, Si, and Ti present on the surfaces of the materials used in this study. The surface morphology of biochar at different conversions (as reported in Papers I and II) was investigated using a Zeiss GeminiSEM 450 at 15 kV, which was coupled with EDX (energy-dispersive X-ray spectroscopy). The concentration of surface elements was determined using a Si (Li) detector and the Oxford INCA Energy program. The samples were analysed in low vacuum mode with carbon tape beneath them. In Paper V, SEM-EDS measurements were taken after gasification for a few minutes in 15% CO_2 at 900 °C, resulting in a degree of char conversion of around 30%. The morphology of the wood char surface was distinguished from that of the straw surface using SEM (Phenom ProX Quanta 200 FEG).

3.2.5 Data analysis

The following parameters were calculated and used in the studies to analyse the char gasification stage.

Char conversion is a term derived from the curves of mass loss as shown in Equation 3-1. Instantaneous reactivity (R) was calculated according to Equation 3-2.:

$$X = \frac{m_0 - m_t}{m_0 - m_{ash}} \ [-] \qquad 3\text{-}1$$

$$R = \frac{dX}{dt} = -\frac{1}{m_0 - m_{ash}} \frac{dm_t}{dt}, \qquad [\mathrm{min}^{-1}] \qquad 3\text{-}2$$

Where m_0 represents the initial mass of the char at the onset of gasification, m_t is the instantaneous mass of the char at time t, and m_{ash} is the remaining mass of ash. The K/C mole ratios during the conversion process were determined as follows: the C content throughout the conversion was determined by analysing the mass loss rate multiplied by the fixed carbon content, while the K content was determined based on the bulk potassium content. TGA was used to study the intrinsic char reactivity of different chars.

Paper VI used an additional data analysis method. To obtain the calculated sample mass of wood and straw mixtures (m_{cal}) at a given time t, the results for pure wood and straw at a specific reaction time were used, and the following formula was employed:

$$m_{cal} = m_w f_w + m_s f_s \qquad 3\text{-}3$$

where m_w and m_s represent the wood and straw masses at a time t, and f_w and f_s represent the initial fractions of the wood and straw mixture.

In a similar way, the calculated alkali release rate (i.e., theoretical alkali release rate, A_{cal}) of the mixtures at time t was obtained using the following equation:

$$A_{cal} = A_w f_w + A_s f_s \quad 3\text{-}4$$

where A_w and A_s represent the instantaneous alkali release rate for wood and straw, respectively.

The synergistic effects observed at a particular conversion ratio X during the isothermal co-gasification process can be expressed by a synergy index (*SI*) [31,32,117]:

$$SI = \frac{t_{X,cal}}{t_{X,exp}} \quad 3\text{-}5$$

where $t_{X,cal}$, and $t_{X,exp}$ denote the calculated and experimental gasification time required to reach a conversion ratio X, respectively. When the value of *SI* is larger than one, it indicates a positive synergistic effect during co-gasification, and a higher *SI* value indicates a more significant synergistic effect [31].

3.2.6 Kinetic modelling

Paper II discussed gasification kinetics. The kinetics of gasification are generally described as a combination of the effects of operating conditions and char conversion. Equation 3-6 represents the kinetics of a reaction [118,119]:

$$\frac{dX}{dt} = k(T) * g(p_g) * f(X) \quad 3\text{-}6$$

$k(T)$ is the apparent reaction rate constant and the $g(p_g)$ function indicates the dependence of the reactivity on the partial pressure of the gasifying agent. X is the conversion and $f(X)$ describes the structure change, which is dependent on the conversion. The partial pressure (p_g) of the gasifying agent was kept constant.

The reaction rate constant is only temperature dependent and can therefore be defined by the Arrhenius equation (3-7).

$$k = k_0 exp\ (-\frac{E}{RT}) \quad 3\text{-}7$$

k_0 is the pre-exponential factor, E is the activation energy (J/mol), R is the universal gas constant (J/mol/K), and T is the reaction temperature (K).

Four models were used to describe the steam gasification rate of the char samples, namely, a first order pseudo-homogeneous model (HM), a shrinking core model (SCM), a random pore model (RPM) and a modified random pore model (MRPM).

In the HM [120] the first order reaction rate is proportional to the conversion. The model assumes that the steam reacts with the char at active sites that are uniformly distributed throughout the particle. Structural changes during the reaction are not taken into consideration. The expression for reactivity according to HM is shown in 3-8.

$$\frac{dX}{dt} = k_H(1 - X) \quad 3\text{-}8$$

Szekely and Evans [121] proposed SCM model, assuming that a particle has a uniform nonporous structure and that the reaction takes place on the external surface. If the reaction is under chemical reaction control and the shape of the grain is spherical, the overall reaction rate is shown as:

$$\frac{dX}{dt} = k_s(1 - X)^{2/3} \quad 3\text{-}9$$

The RPM model developed by Bhatia and Perlmutter [122] assumes that reactions happen both on the external surface and in the pores. The pores coalesce and new pores generate simultaneously as the carbon is consumed. The RPM expression is given below [122]:

$$\frac{dX}{dt} = k_r(1 - X)\sqrt{[1 - \psi \ln\ (1 - X)]} \quad 3\text{-}10$$

Where ψ is known as the structure parameter, related to the pore structure of the non-reacted sample. It can be determined by the experimental maximum conversion values ($0 \leq X_{max} < 0.393$) according to [121,123]:

$$\psi = \frac{2}{2\ln(1 - X_{max}) + 1} \qquad 3\text{-}11$$

A modified model was developed based on RPM to describe the catalytic activity of the ash compounds [67,124]. According to this model two empirical constants are introduced:

$$\frac{dX}{dt} = k_r(1 - X)\sqrt{[1 - \psi \ln(1 - X)]}\,(1 + (cX)^p) \qquad 3\text{-}12$$

c and *p* are dimensionless parameters used to describe the observed increase in the reaction rate due to the catalytic activity of the mineral content [67]. Throughout the paper, this model modification is called the modified random pore model (MRPM).

Equations (3-8), (3-9) and (3-10) are linearized, resulting in the equations (3-13), (3-14) and (3-15), allowing the determination of the reaction rate constants at different temperatures from the slopes of the linear expression.

$$k_H t = -ln(1 - X) \qquad 3\text{-}13$$

$$k_s t = 3\left[1 - (1 - X)^{1/3}\right] \qquad 3\text{-}14$$

$$k_r t = \frac{2}{\psi\left\{\sqrt{[1 - \psi ln\,(1 - X)]} - 1\right\}} \qquad 3\text{-}15$$

It should be noted that ψ depends on the initial structural properties of chars [122]. It can be derived from the maximum conversion rate given in Equation (3-11).

Chapter 4

Porous structure development and the effects of alkalis

Char pore structure and the presence of alkali and alkaline earth metals are two key parameters that can affect char reactivity. However, most studies of steam biomass char gasification focus on either char structure development [63,125] or ash content [35,64,70,126,127], neglecting the combined effect of both parameters. Mechanistic studies of how both parameters contribute to the reactivity of char during its transformation under steam gasification conditions are important to enable the development of kinetic models.

This chapter summarizes the work conducted in Papers I and II investigating the steam gasification of commercial gasifier char. It describes the development of the porous structure and potassium-induced phenomena.

4.1 Effect of porous structure development on char reactivity

In this section, the aim is to study the effects of porous structure development on the steam gasification reactivity of commercial biochar residues at different temperatures using a TGA instrument. The biochar was partially gasified and characterized in terms of textural and morphological characteristics, as well as ash content. The ash-leached char samples were also compared with the original char to evaluate the combined effects of structural development and ash effect.

The micropores development reactivity of char and the pore size distribution of char at different conversions at 800 °C are shown in Figure 4.1 (results for 700 °C and 750 °C can be found in Paper I). Figure 4.1a shows there are two distinct regions of conversion with different reactivity behaviour. The ratio curve between the micro surface area and total specific surface area (S_{micro}/S_{total}) shows a close correlation with changes in reactivity. In the conversion range from 0 to 70%, both reactivity and the S_{micro}/S_{total} ratio decreased. Thereafter, the reactivity starts to increase similarly to the S_{micro}/S_{total} ratio. This behaviour may be related to the generation of new micropores, resulting in an extended surface area for heterogeneous steam-carbon reaction, which leads to increased reactivity.

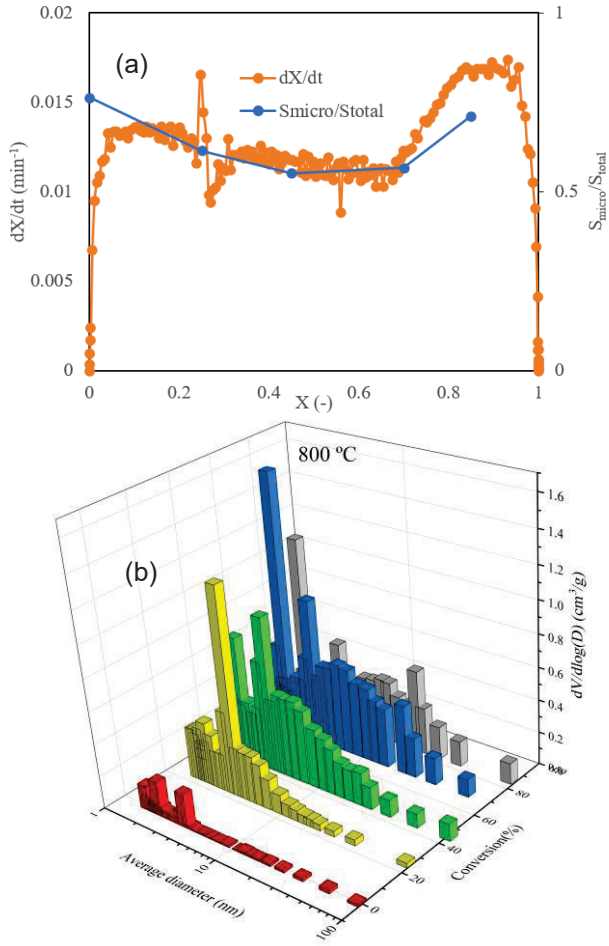

Figure 4.1 (a) Micropore development and reactivity at 800 °C; (b) Pore size distribution of char at different conversions at different temperatures according to the Barrett-Joyner-Halenda (BJH) method.

As shown in Figure 4.1b, micropores are generated simultaneously with the growth of mesopores (2–50 nm) during char conversion. This process also results in the development of macropores (> 50 nm) at higher conversions, although to a lesser extent. The simultaneous and uniform development is indicative of a porous network [8] that is interconnected. When the conversion rate exceeds 70%, the mesopores fraction begins to decrease while macropores show progressive pore growth. It's worth noting that the pore volume in the macropore range exhibits a positive correlation with the conversion rate.

As shown in Figure 4.2, the total pore volume (V_{total}) and the total specific surface area (S_{total}) increase 1.3–3.1 and 2.0–5.3 times, respectively, with conversion up to about 70% at all temperatures. This indicates formation of new pores as a result of

steam-carbon reaction. Similar results are reported in other studies [63]. S_{total} and V_{total} start to decrease after about 70% conversion. The fraction of micropores increases with conversion monotonically and constitutes most of the surface area of the char. The generation of micropores suggests a reaction on the active sites of char on the external surface [128] or the opening of the closed pores of the biochar structure [66,129]. Both possibilities are supported by the observed increase in char surface area and pore volume (Figure 4.2). More details can be found in Paper I.

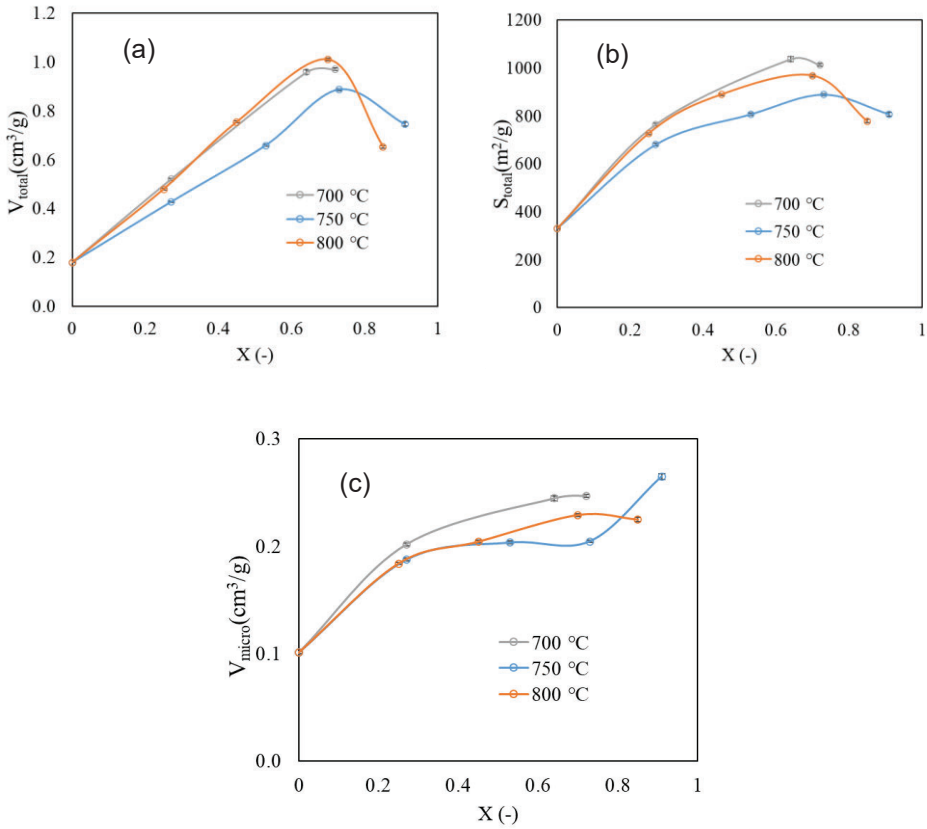

Figure 4.2 Textural properties of the OC at different temperatures: (a) the total pore volume versus conversion; (b) the total specific surface area versus conversion; (c) the micropore volume versus conversion.

The SEM images (with 1000× magnification) of original char and gasified chars at different carbon conversions from gasification at 700 °C are shown in Figure 4.3. The surface of the original char is quite porous with sparse mineral particles, mainly Ca, distributed thinly on the char surface. Carbon is continuously consumed during the gasification reaction, and pores of gasified chars expand and increase resulting in the formation of honeycomb-like structures on the char surface. At 25% char

conversion, the surface is more porous than the original char, with a greater number of small pores dispersed across the surface scattered on the char surface. During the char conversion, the initial holes are enlarged and new pores are produced (circled in red), while the particle size of the char steadily decreases. Consistent with the findings of Yonghui et al. [6–8], agglomerates are generated at higher conversion (green triangle) due to the increased mineral content during char consumption. More detailed information on the char SEM gasified at 750 and 800 °C can be found in Paper I.

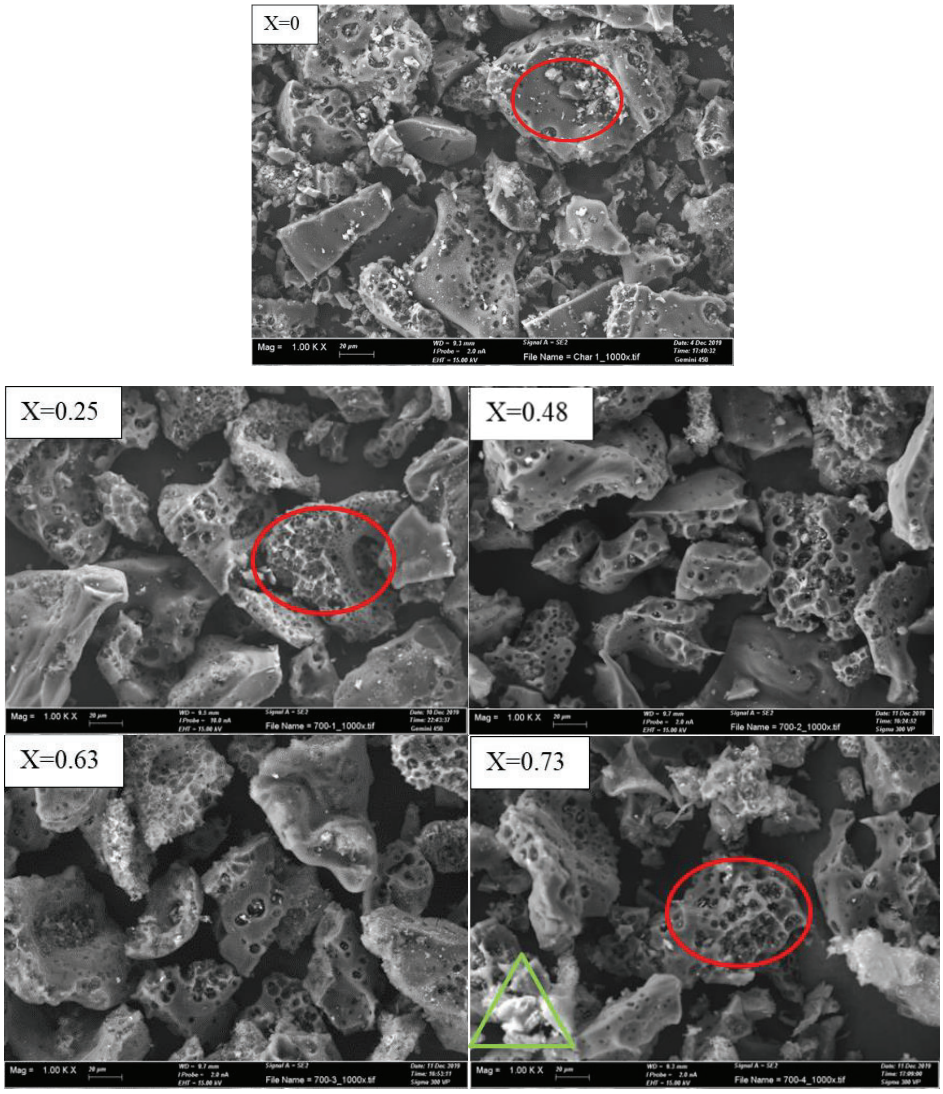

Figure 4.3 SEM images (1000× magnification) of char with different carbon conversions prepared from char gasification in H_2O at 700 °C.

4.2 Effects of alkali on char reactivity

This section describes the findings related to the catalytic effects of alkali in the steam gasification of char with varying intrinsic mineral contents but a similar morphology. The aim was to enhance understanding of the effects of minerals on the kinetics of steam gasification. Different kinetic models were employed to validate the steam gasification activity results.

Figure 4.4 depicts the instantaneous reactivity (R) of all samples as a function of the conversion at 700 and 800 °C. As shown, the R of all the samples is essentially the same until a certain degree of conversion, followed by a rapid increase as conversion progresses. At degrees of conversion below 0.6 at 700 °C, the observed difference in R for the three chars at the same temperature is small with a subsequently faster increase in R with higher potassium contents (Figure 4.4a). The onset varies with the degree of leaching (differing potassium content) and is observed at conversions of 67%, 78% and 92% for the OC, 2LC, and 48LC biochars respectively.

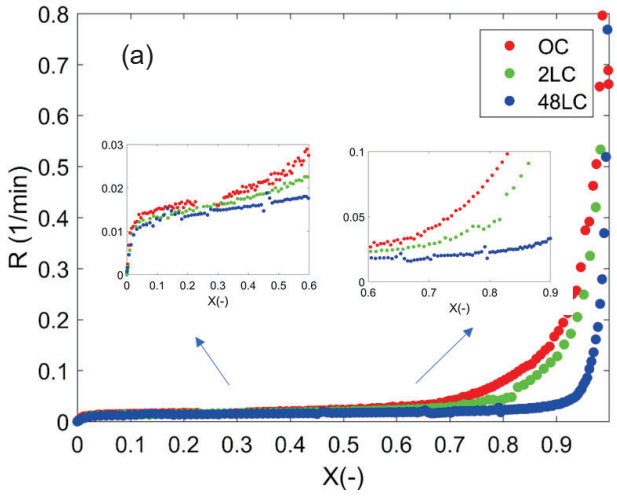

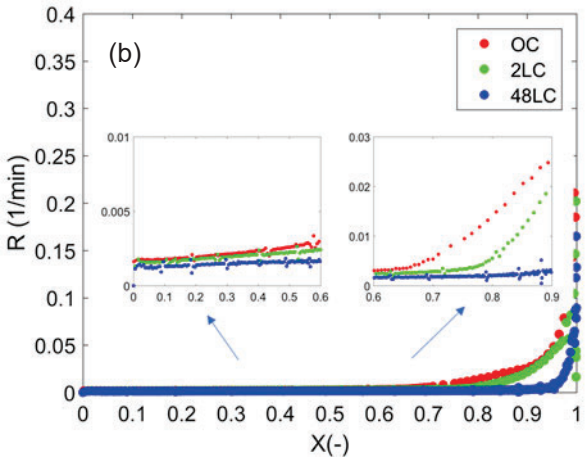

Figure 4.4 Instantaneous char gasification rates of all samples at (a) 700 °C and (b) 800 °C as a function of the degree of conversion.

At higher temperatures the onset is shifted to a lower degree of conversion, as illustrated for OC and 48LC at 800 °C in Figure 4.4b, but with the same order between the chars. The shift due to the higher temperature is rather small in the case of 48LC, indicating that potassium is the main reason for the larger shift observed for OC and 2LC. At a temperature of 800 °C, the instantaneous rate of conversion sharply increases during the initial stage, as depicted in Figure 4.4b (left insert).

The leaching process removes material uniformly throughout the particle volume, as similar proportions of aluminium, calcium, and potassium content in both the bulk and surface of carbon particles between 2LC and OC was observed. This supports the hypothesis that potassium volatilization is negligible. More information can be found in Paper II. Although the quantity of potassium is linked to the reactivity of the char, its distribution, composition, and coverage by carbon are also crucial factors. It has been reported that potassium silicates and/or aluminates that are formed during gasification have no catalytic activity for char conversion [18,21,70,130,131] and additionally act as a diffusion barrier for the oxidizer [132]. However, X-ray elemental mapping of char surfaces indicates that the formation of silicates or aluminates is negligible and thus the total amount of potassium can be considered as active. The dispersion and the surface coverage of potassium is also an important parameter to consider when considering the activity of potassium. The ratio K/C was used to address the surface availability. The calculation method can be found in section 3.5.2.

Figure 4.5 shows *R* as a function of K/C for the different char samples for 700 °C. The reaction rates slowly increase (relative change < 25 %) for K/C ratios less than

5×10^{-3} with the corresponding conversion being lower than 70% (see also Figure 4.6). This suggests that the earlier stage reactions are noncatalytic. When the K/C ratio is larger than around 5×10^{-3} there is an obvious monotonic increase of the reaction rate for all temperatures. This indicates that there is a critical value of active site availability for the conversion above, which is greatly influenced by the potassium present. A closer look at 700 °C in Figure 4.5 shows that *R* follows a monotonic increase until complete conversion (X > 90% and K/C > 0.02). The only exception is OC, where the increase rate of the *R* diminishes as complete conversion approaches. Finally, no inflection point was observed for the K/C ratio at which the *R* begins to decrease, unlike in the gasification of high-ash-containing char [18,133–135]. The different behaviour, compared to the literature may be due to the difference in ash content between agricultural char and woody char. Agricultural chars typically have much higher silicon content than wood, and silicon is widely known to be a catalyst deactivator [21,70,131] due to its strong thermodynamic affinity for potassium. Physically, a molten layer around the fuel particles might restrict gas agent transfer. The result indicates that surface saturation is sample-specific (ash-K loading) and depends on the temperature history of the char.

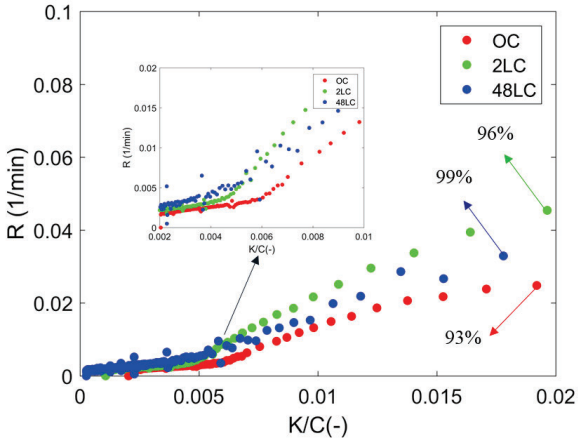

Figure 4.5 *R* versus the atomic K/C ratios from 0 to 0.02 for 700 °C.

Four different models were used to model the experimental results. The results are shown in Figure 4.6. The HM model fails completely, especially for the higher temperatures 750 °C and 800 °C. The SCM model was better, but the RPM model provides a still more satisfactory description of the degree of conversion, depending on the K content and the temperature. However, while the RPM model reconstructs the gasification curve up to a conversion of 70%, it does not adequately account for the increase in reaction rate related to the catalytic effect of ash beyond this point. To address this issue, the MRPM model was implemented to describe the specific catalytic effects of potassium on char gasification. It was found that this model could

describe the entire conversion process, including the observed peaks in reactivity, for all cases. The first peak, potentially associated with the role of water-soluble calcium in promoting pore development, is explained by the role of the dispersion and form of calcium species in enhancing the porous structure of the char [136]. The second peak, ascribed to the catalytic effects of potassium, is also captured by the MRPM model for all cases.

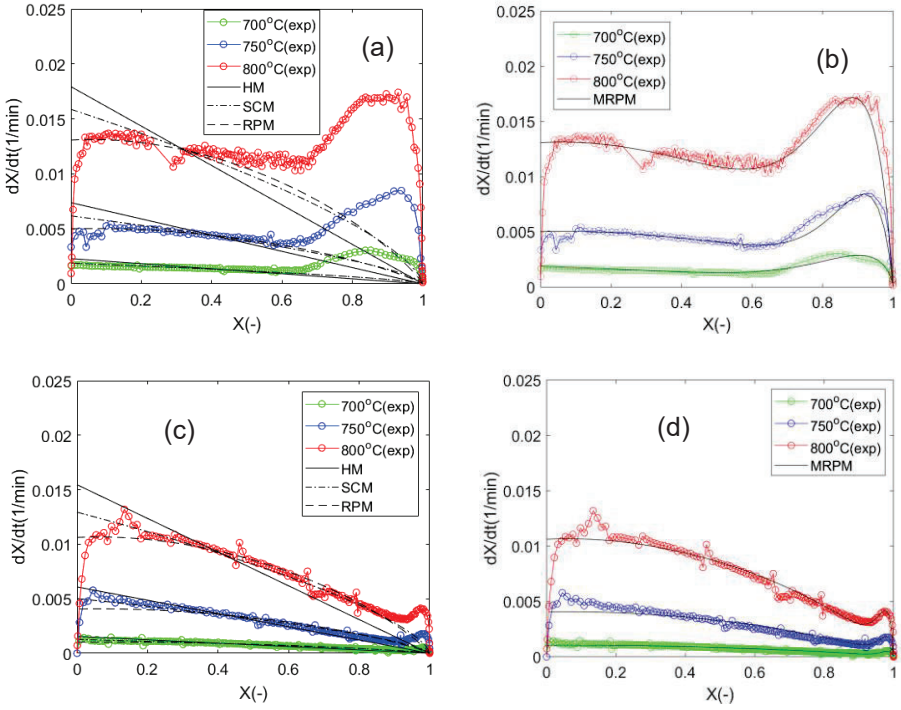

Figure 4.6 Comparison of the simulated and experimental data for gasification of (a) (b) OC, (c) (d) 48LC.

The factors *c* and *p* (Equation 3-12) are two derived parameters in MRPM related to the inorganic content in the char [67]. Figure 4.7 shows a linear increase in *c* with increasing K concentration, while *log(p)* exponentially decreases for all temperatures. Zhang et al. [67,137] reported similar results for *c* when they investigated steam gasification of chars from different biomasses at 850 °C and coal and carbon at 900 °C. In both those studies, a single temperature was used in the char gasification experiments. In this study, the parameter *c* was found to be independent of the measured temperature range, as disclosed by the well separated points at each K concentration. The *p* parameter also strongly depends on the potassium content and shows a small negative correlation with temperature. Nevertheless, the exponential decrease of *log(p)* versus K concentration differs from the results reported by Zhang et al. [67,137], who observed a linear decrease. The reason for this is currently unclear and further investigations is needed.

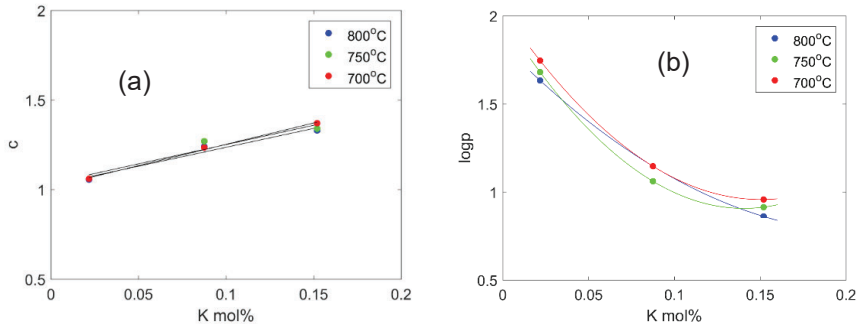

Figure 4.7 Relationships between potassium concentrations and the empirical constant (a) *c* and (b) *p* in the MRPM (trendlines as a guide for the eye).

Chapter 5
Alkali release behaviour

The importance of alkalis in gasification processes and their effect on char reactivity was well established in chapter 4. Knowledge of the behaviour of alkalis during biochar gasification is currently limited, with only a few studies contributing to understanding the mechanism at work. In particular, only a limited number of studies have investigated the release of alkalis as a function of char conversion during steam [23,24] and CO_2 [20] gasification, and all of them have focused exclusively on agricultural biochar.

In this chapter, the aim is to shed light on this issue by characterizing the release of alkalis during woody and agricultural biochar conversion under both CO_2 and steam conditions (Paper III and IV). Alkali release was investigated with high temporal resolution, and the results relate the alkali behaviour to char conversion rate.

5.1 Alkali release behaviour during CO_2 gasification

This section presents the results for alkali release and char reactivity during CO_2 gasification. Five diverse types of biomass chars were used as feedstock: furniture waste, straw, pine, wood and branches, and industrial char. The experiment was performed by using an online alkali measurement setup with TGA (Figure 3.1). Mass loss and alkali emission were monitored simultaneously, facilitating a correlation between the two parameters. The impact of CO_2 concentration, gasification temperature, and char production method on the results is described and discussed.

5.1.1 Reactivity and alkali release

Figure 5.1 displays the mass loss rate, alkali release rate, and reactivity of four types of biomass-based samples during CO_2 gasification. For all samples, the mass loss rate increases immediately when CO_2 is injected (Figure 5.1a). The pine and furniture waste chars are gasified at a similar rate, while the gasification of wood and branches char is substantially faster. Straw char has a different profile with a continually decreasing conversion rate as the conversion ratio increases (Figure 5.1a and 5.1c). Wood-based chars undergo three stages: a rapidly decreasing conversion rate (*r)* at a low conversion ratio followed by a stage with a slowly decreasing *r* and finally an increasing *r* before conversion is completed (Figure 5.1c).

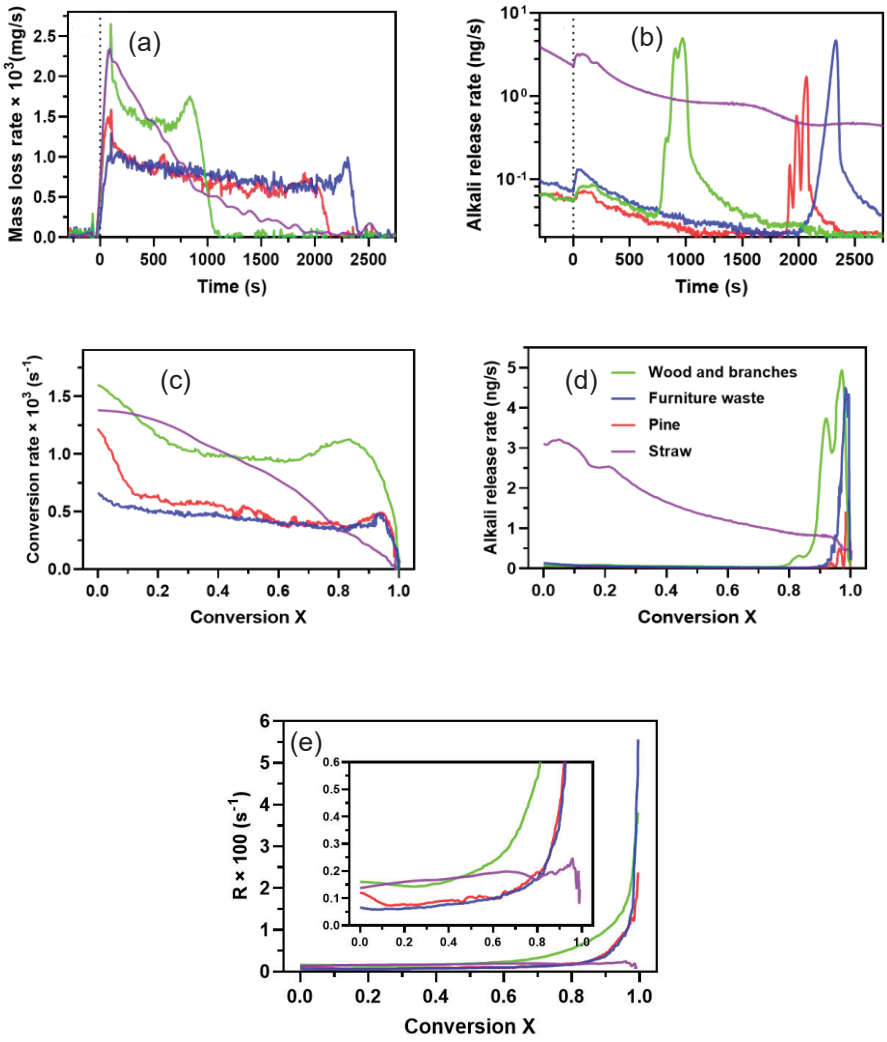

Figure 5.1 Sample mass and alkali release rate during CO_2 gasification of char produced from pine wood, a mixture of wood and branches, furniture waste, and straw: (a) sample mass loss rate; (b) alkali release on a logarithmic scale; (c) conversion rates; (e) instantaneous reaction rate *R*; (d) alkali release rate as a function of conversion ratio.

The mixture of wood and branches has a higher char reaction rate compared to pine and furniture waste due to higher potassium concentrations (Table 3.1: 1430, 530, and 340 mg/kg, respectively). Therefore, differences in reactivity follow the expected trend of the alkali concentration in the original materials. The behaviour of straw char is distinct from that of woody chars. Although its high potassium concentration (7790 mg/kg) suggests increased reactivity, its abundance of silicon

(6610 mg/kg) and phosphorus (260 mg/kg) has a detrimental effect on char reactivity [22,138]. The formation of K-rich silicates and phosphosilicate likely immobilizes alkali, reducing their availability for catalytic reactions. However, a possible stabilization due to a higher concentration of calcium may partly hinder the deactivation of alkali [79]. These findings are consistent with previous observations [5,126,127] of a correlation between gasification reactivity and potassium content in steam gasification.

As shown in Figure 5.1b, alkali release increases when CO_2 is injected and then decreases for all forms of char in a similar way. The absolute alkali release rate is comparable for wood-based chars, but for straw char it is 40–50 times higher due to the high alkali content. As gasification approaches completion, all three wood-based chars display a remarkable increase in alkali release rate of up to two orders of magnitude. The peak is followed by a rapidly decreasing alkali emission from the remaining ash. The alkali emission from straw ash behaves markedly differently, for the release rate decreases continuously to the end of the gasification process.

As shown in Figure 5.1d, the alkali release from straw char reduces progressively with increasing conversion ratio and can be approximately proportional to the amount of remaining char mass. For the wood-based chars, they showed similar patterns of alkali release during gasification. The alkali release increased when the gasification began and then slowly decreased as the process continued, until a significant release of alkali occurred as gasification neared completion. This pattern has also been observed for potassium-loaded coal char. Halim et al. [134] conducted a study on lignite char samples with varying potassium content and found that while there was no volatilization of potassium at low conversion levels, there was a noticeable loss of potassium for $X > 0.7$. These results suggest that alkali is gradually enriched in the char during gasification and is finally released in large amounts under the conditions present during the final stage of the process. This interpretation aligns with observations of increasing alkali concentrations in biochar as conversion increases [23,24].

The final peak in alkali release observed for woody chars is likely related to an increase in instantaneous char reaction rate. The increase in rate is believed to be due to a significant catalytic effect of alkali caused by the formation of more active C-K sites (see Figure 5.9). A detailed mechanism will be presented in section 5.3. The effect of CO_2 concentration, temperature, and char production method on alkali release and char reactivity supports this conclusion. Specifically, high CO_2 concentration and high gasification temperature both result in increased alkali release and char reactivity, as discussed further in the next section.

5.1.2 Effects of operating conditions and char production method

The influence of temperature and CO_2 concentration on gasification reactivity and alkali release is illustrated in Figure 5.2. A high CO_2 concentration increases the char gasification reactivity and increases the alkali release rate (Figure 5.2a) as the char is consumed. Temperature is another important parameter: a high temperature is expected to accelerate the gasification process [35]. As shown in Figure 5.2b, the reactivity (R) of the pine char increases significantly with increasing temperature during all stages of the gasification process, with the reactivity nearly doubling at 950 °C compared to 900 °C. A higher gasification temperature also results in a higher alkali release rate, as shown in Figure 5.2c. For $X < 0.8$, the alkali release rate increases slightly when the temperature is raised from 850 °C to 900 °C, and then substantially as the temperature is further increased to 950 °C.

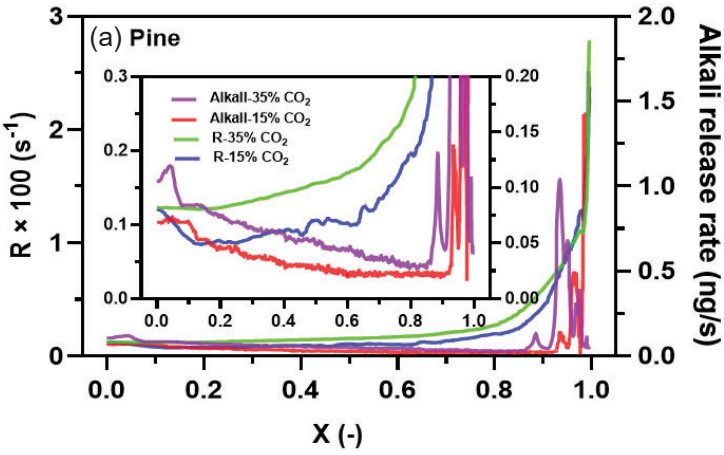

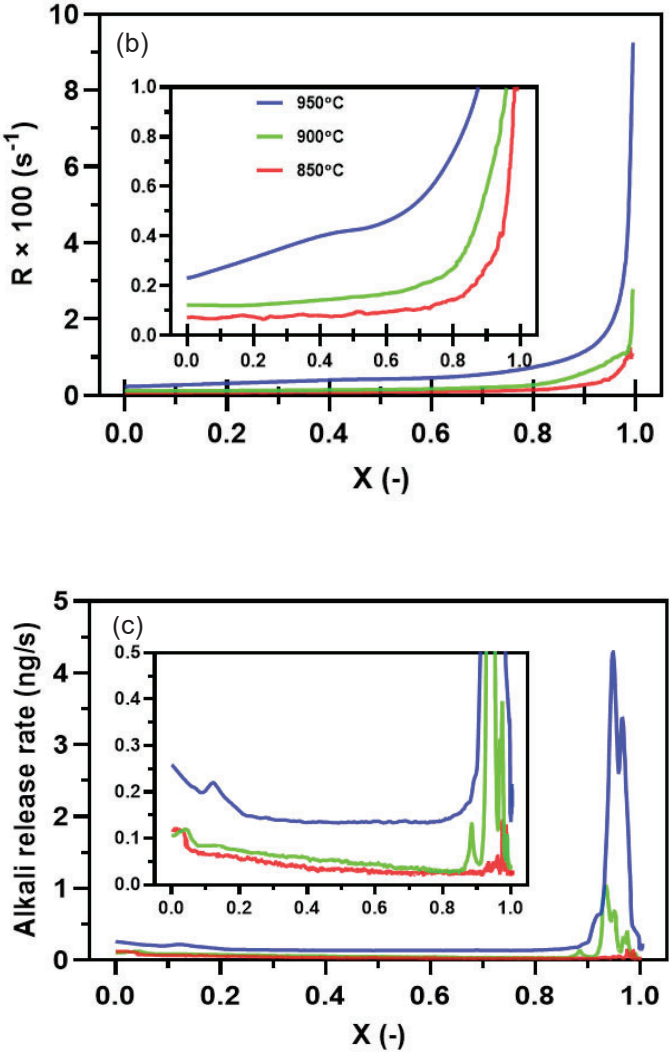

Figure 5.2 (a) Instantaneous conversion rate and alkali release rate as a function of conversion ratio in 15% and 35% CO_2 for pine; (b) conversion rates and (c) alkali release rate as a function of conversion during pine char gasification in 15% CO_2 at 850 °C, 900 °C, and 950 °C. Legends for panel (c) are the same as in panel (b).

A high CO_2 concentration and a higher temperature can both enhance the R and alkali release. There is, however, not a one-to-one relation between the two parameters. Over a large conversion range ($0 < X < 0.6$), the instantaneous conversion rate slowly increases while the alkali release rate decreases. This suggests that the processes are complex and that other factors are at play in addition

to the catalytic effect of the available alkali. These factors may include, char structure and the influences of other minerals [20,21].

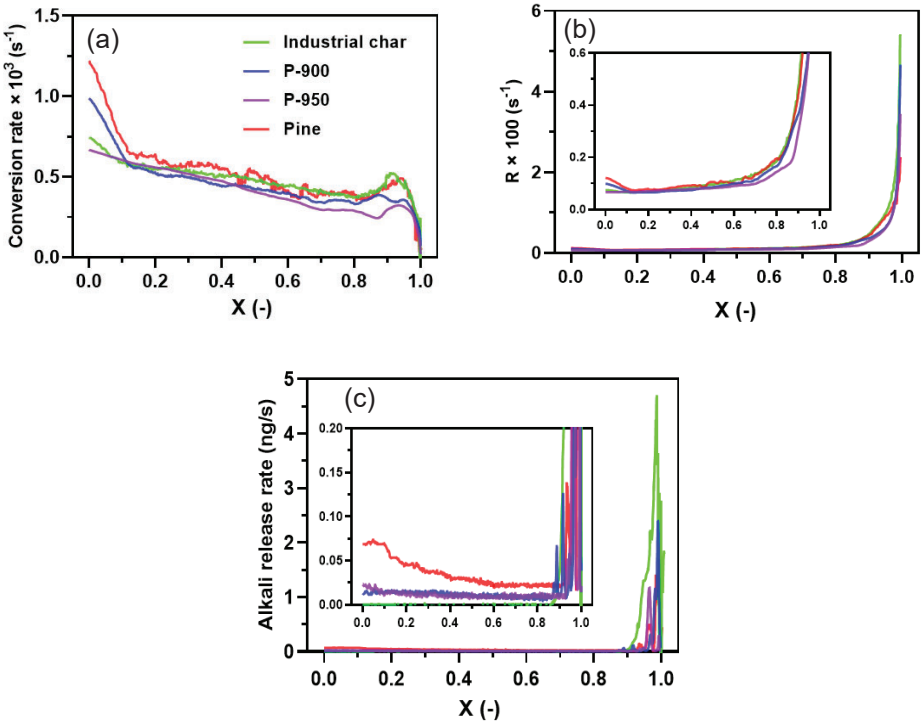

Figure 5.3 Conversion of pine char samples obtained from different char production processes during gasification in 15% CO2 at 900 °C: (a) conversion rate; (b) instantaneous conversion rate (*X* from 0 to 0.995); (c) alkali release rate.

Studies focusing on pine char also illustrate the influence of the char production method. Typical results are presented in Figure 5.3. The chars produced with intermediate cooling processes in TGA (P-900: pretreated at 900 °C and cooling to 200 °C; P-950: pre-treated at 950 °C and cooling to 200 °C) have lower gasification reactivity than the standard pine sample (Figures 5.3a and 5.3b), with noticeable differences in the initial and final conversion stages. The alkali release from the pine sample is also significantly higher than that from the intermediate cooling char. Clearly, heating and cooling the samples reduces the amount of alkali available for release during the subsequent gasification procedure. Therefore, the enhanced stability of alkali compounds within the char structure could be considered as a possible explanation for the decreased release found for intermediate cooling chars. Structural changes in the char [83], and alkali reactions with other compounds (e.g. SiO_2) may both play a role in producing more stable alkali compounds. The industrial char (IC) sample was collected from an industrial entrained flow gasifier

that used the same pine wood as fuel. Samples experienced gasification temperatures up to 1200 °C in the industrial process. The observed IC conversion rates are similar to the results for the other three samples.

5.2 Alkali release behaviour during steam gasification in a fixed bed reactor

This section describes the finding from studies of the release of alkali substances from various biochars using steam as an agent (Paper IV). An industrial char (IC) sourced from an entrained flow gasifier was studied to assess its alkali release behaviour at temperatures ranging from 800 °C to 950 °C and for two different particle sizes. The study results were compared with those from two other biochars to gain further insights into the relationship between char and alkali interactions. The study employed a fixed bed system, as shown in Figure 3.2.

5.2.1 Alkali release of biochar

Figure 5.4 shows that the alkali release concentrations gradually rise until they reach a maximum point consistent with the CO and CO_2 maximum peak in the later stage. It is important to note that a fixed bed with a height of 10 mm is being used. At the beginning of the char conversion, the alkali desorbs from the particles in the conversion zone, moves upwards in the bed, and becomes trapped by interacting with the char located at the top of the bed. The peak of alkali release observed at the end stage of gasification may be due to free alkali that can no longer be adsorbed onto the char particles, since the bed has almost disappeared, as well as alkali that is released from the final shrinking char particle present in the bed. Furthermore, the alkali catalytic effect is more dominant towards the end stage of char conversion. As the char conversion nears its end, with only a thin layer of char left in the bed, the catalytic effect of alkali becomes significant due to the rapid formation of more active sites [5] as the K/C increases.

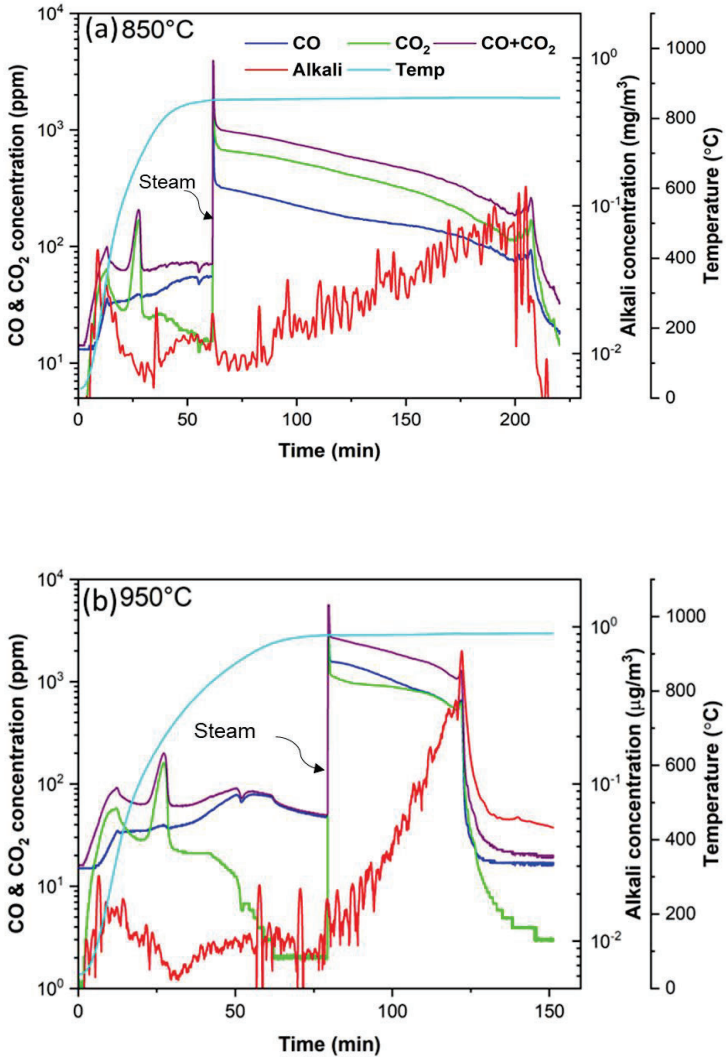

Figure 5.4 CO, CO_2 and alkali concentrations as a function of time during heating and subsequent steam gasification of industrial gasifier char at 850 °C and 950 °C.

High temperature creates favourable thermodynamic conditions and accelerates the reaction kinetics [35]. Figure 5.5a and 5.5b demonstrate that the reactivity (r and R) of industrial char increases significantly throughout the gasification process as the temperature rises. At 950 °C, reactivity is nearly twice as high as at 900 °C. Moreover, at all temperatures, the R value increases exponentially during the later stages of gasification.

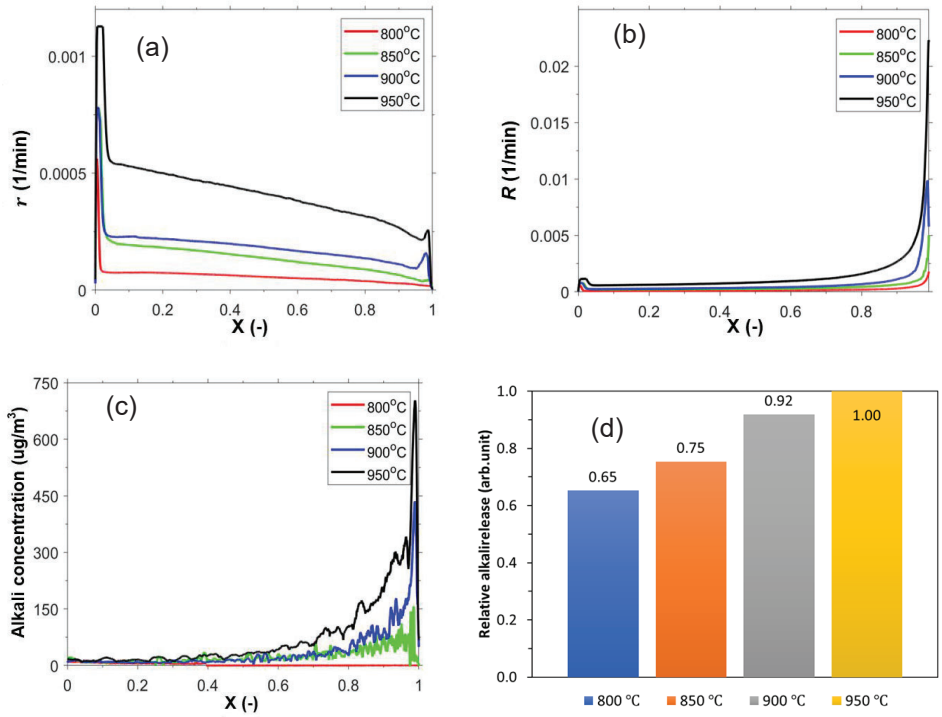

Figure 5.5 Reactivity and alkali release of industrial char at different temperatures: (a) Conversion rates versus conversion; (b) *R* versus conversion (*X* from 0 to 0.99); (c) alkali release versus conversion; (d) normalized alkali release.

Alkali release of IC versus conversion at different temperatures is shown in Figure 5.5c. In the char gasification process, the alkali release is divided into two stages. When conversion $X < 0.6$, the alkali release increased monotonically. When, $X > 0.6$, alkali begins to release exponentially until the gasification process is complete. The more char is converted, the more alkali is migrated/exposed on the char surface and then released [139]. A higher gasification temperature resulted in a higher alkali release because at a higher temperature the desorption of the alkali is faster and can accelerate the decomposition of inorganic alkali compounds [140]. This is consistent with previous studies under CO_2 conditions (section 5.1.2). As shown in Figure 5.5d shows that at 950 °C the alkali release is 35%, 25%, 8% higher than at 800 °C, 850 °C and 900 °C, respectively.

5.2.2 Effect of particle size

Further information was obtained through studies involving different char particle sizes. Two particle sizes with diameters of 125 and 235 μm were examined, with specific surface areas of 221 and 172 m^2/g, respectively. As shown in Figure 5.6a and 5.6b, the smaller char particle size demonstrated higher char reactivity, which is

consistent with other studies [141–143]. The increase in reactivity with decreasing particle size may be attributed to a reduction in diffusional resistance for steam into the char particles [143]. This indicates that for the particle sizes examined in this study, diffusion restrictions cannot be neglected for industrial char. These findings align with previous investigations [141,142].

The alkali release data obtained from experiments involving different particle sizes also supports the above observations. As shown in Figure 5.6c, alkali release was more significant for smaller particles than for larger ones, and the final increase in alkali during the conversion process was more prominent for the smaller particles. These trends qualitatively follow changes in char reactivity, which supports the idea of a strong correlation between reactivity and alkali release.

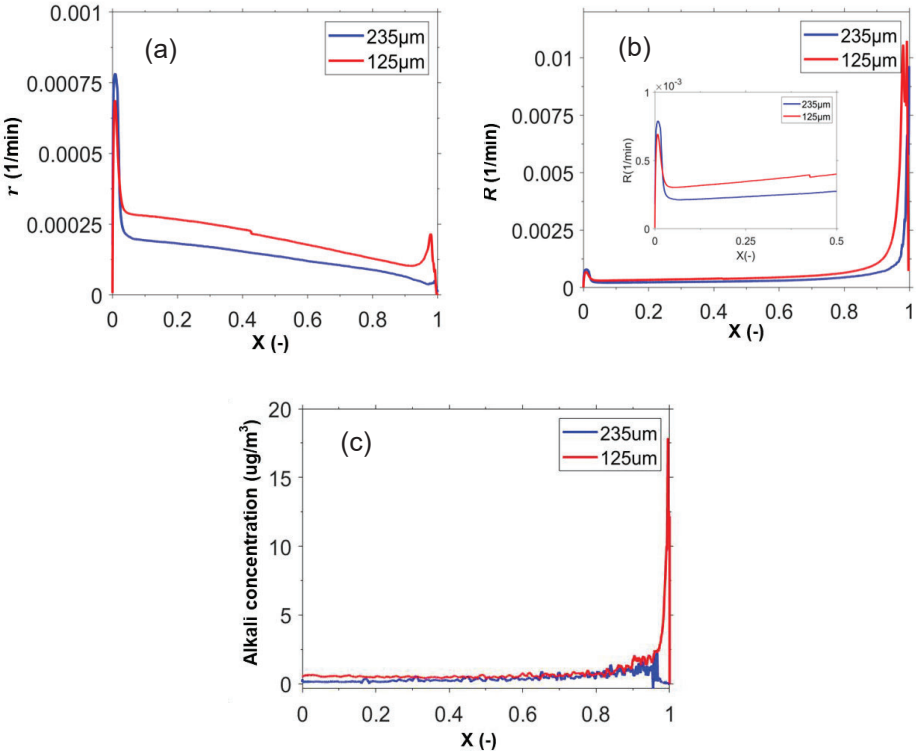

Figure 5.6 Steam gasification at 850 °C of industrial gasifier char with average char particle sizes of 125 µm and 235 µm: (a) conversion rate; (b) instantaneous conversion rate (X from 0 to 0.99); (c) alkali concentration as a function of char conversion. The inset in panel (b) displays the data for X = 0–0.5 in greater detail.

5.2.3 Comparison of different biochar

Results obtained during gasification of the three different char samples are presented in Figure 5.7. For all samples, there are sharp peaks in CO and CO_2

concentrations occur immediately when steam is introduced, indicating a rapid increase in carbon conversion. Three chars showed different gasification behaviours.

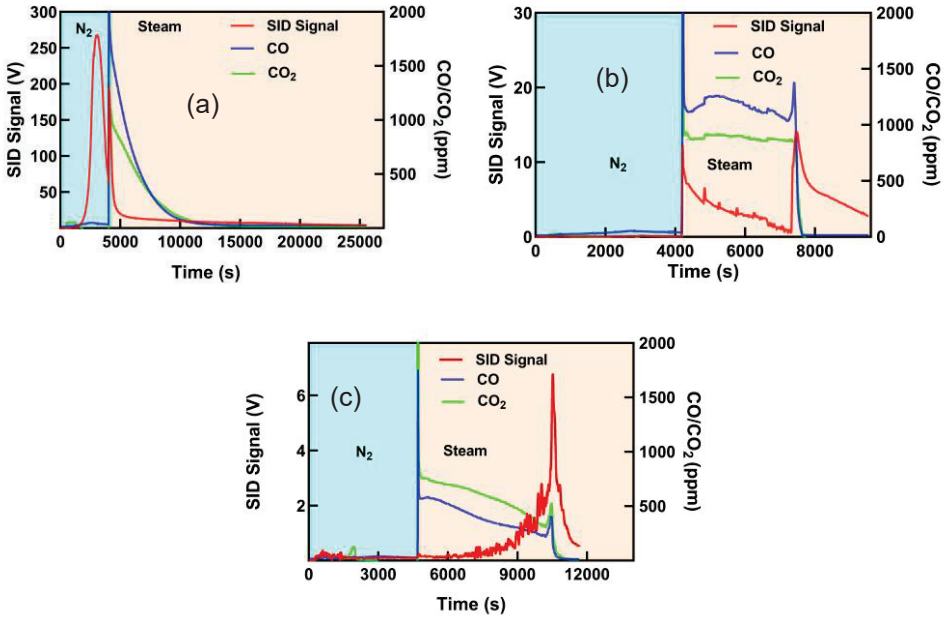

Figure 5.7 Release of alkali, CO_2 and CO for different samples at 900 °C: (a) Furniture waste; (b)Straw; (c)Industrial Char.

In case of furniture waste and industrial gasifier chars, the CO and CO_2 concentrations remain stable or slowly decrease during most of the gasification. However an increase followed by a rapid decrease is observed at the final stage. Furniture waste char exhibits a stable phase that lasts up to 7200 s, while the industrial gasifier char requires 10000 s for the same phase, suggesting a slower carbon conversion rate for the latter. This is also illustrated by the lower reaction rate level for the industrial gasifier char, compared to the furniture waste char in Figure 5.8. The gasification performance of straw char differs significantly from that of woody chars, exhibiting a near-exponential decrease in CO and CO_2 concentrations following the initial reactivity increase caused by the addition of steam. The straw char gasification also takes considerably longer time, indicating a lower overall reaction rate. As can be seen in Figure 5.8, the conversion rate of the straw char starts at a higher rate than that of compared to the woody chars, but thereafter decreases linearly with time.

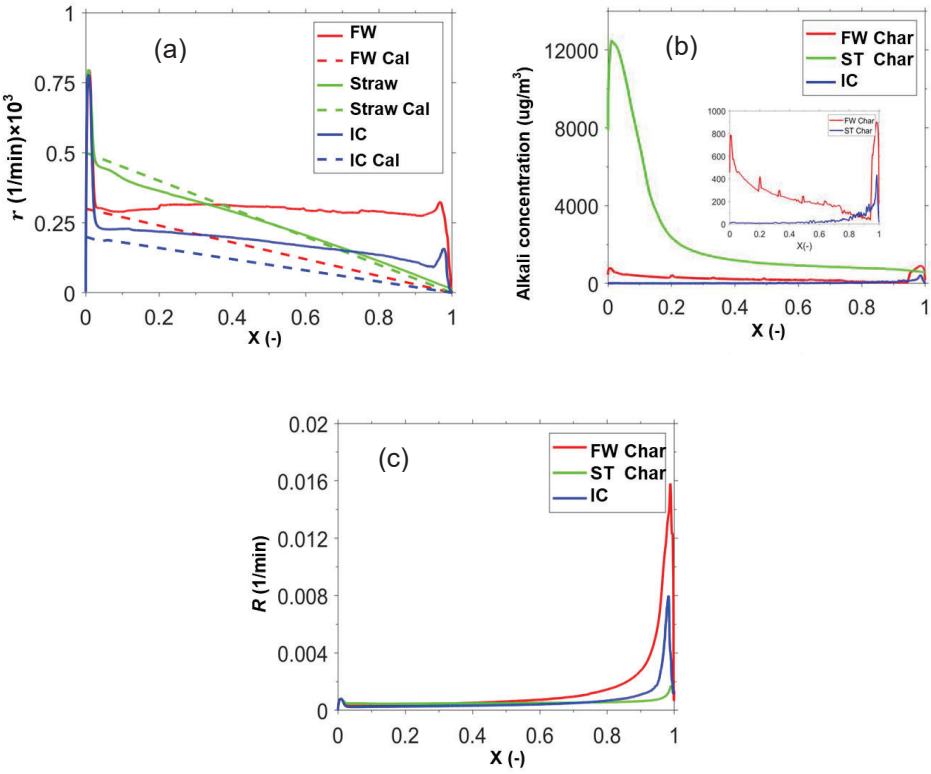

Figure 5.8 (a) Reaction rate r as a function of conversion X for biochars at 900 °C, together with a calculated r (dashed line) assuming a constant mass loss rate after the initial peak; (b) alkali concentration. (c) instantaneous reaction rate R.

The dash lines in Figure 5.8 shows the calculated reaction rate r assuming a constant mass loss rate. It estimated the mass loss data collected directly after the first peak, corresponding to the initial char conversion rate with negligible influence of the gas phase alkali released from converted char. The projected r line for straw char closely follows the experimental r line. By contrast, the experimental reaction rate for woody char largely deviates from the projected lines, exhibiting higher reaction rates throughout char conversion. One possible explanation for the observed behaviour of straw char is that it may be completely saturated with alkali, reaching the maximum rate of alkali-catalysed char gasification, as proposed by Karlström et al. [18]. The observed high alkali release rate supports the presence of alkali in excess on the surface in Figure 5.8b. Nevertheless, other factors might also inhibit the alkali catalytic. When the conversion ratio exceeds approximately 0.3, despite having the highest potassium concentration, straw char exhibits lower reactivity than furniture waste char. This decrease in reactivity may be attributed to the high content of Si (39800 mg/kg) and P (1170 mg/kg) in straw, form K-Ca-rich silicates

and phosphosilicate [144], which are known to reduce char reactivity [22,138]. They immobilize alkali otherwise available for catalytic reactions, although possible stabilization due to the presence of calcium (8330 mg/kg) may partly hinder the deactivation of the alkali [79]. Other studies on steam gasification of biofuels [5,126,127] have reported similar results and shown a similar correlation between gasification reactivity and the potassium fuel content.

5.3 Alkali release and char gasification mechanism

Figure 5.9 presents a simplified schematic model to assist in the discussion of the various factors that affect alkali release and induced alkali catalytic effects. In the diagram, alkalis generally undergo the following processes: (1) redistribution on the biochar surface through diffusion, whereby it diffuses from the bulk to the surface; (2) formation of alkali vapours through desorption or adsorption from existing alkali vapours; (3) migration from one particle surface to another char surface; (4) combination with other metals to form alkali metal silicates; and (5) release through volatilization, which can be measured by SID.

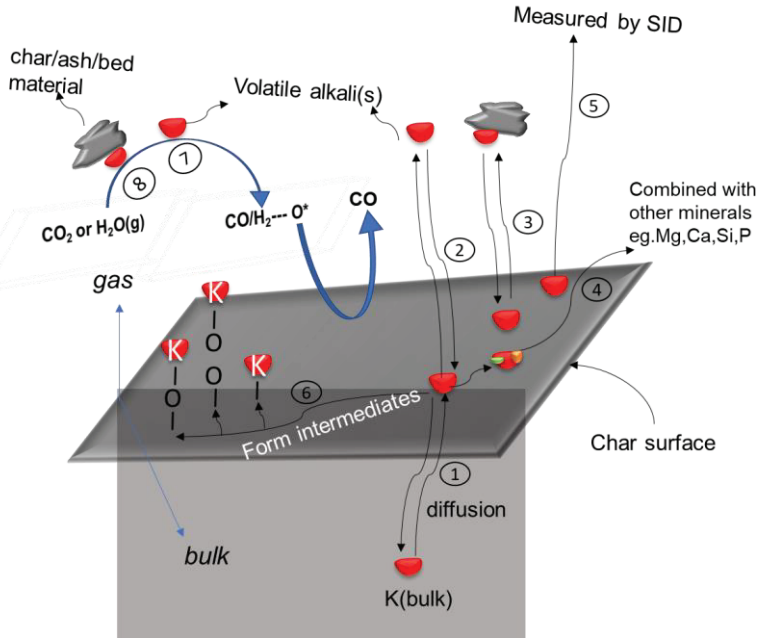

Figure 5.9 Schematics of the alkali release and catalytic mechanism during CO_2 and steam gasification.

The alkali catalytic process can be divided into three parts: (6) carbon–alkali interaction, related to the oxidation of charcoal, forming different intermediates:

carboxylic (–CO_2K), phenolic (–COK) and potassium–carbon (–CK) groups [145,146]; (7) gas–alkali interaction in which the gasification agent (H_2O or CO_2) comes into contact with the gaseous alkali to release more active O* [105]; and (8) interaction between the gasification agent and the alkali present in the ash/bed material, which also releases more active O*.

The different mechanisms of alkali release and char conversion for different biochar particles are shown in Figure 5.10. The different mineral content of woody char (from furniture waste, wood, and branches), straw char, and industrial char may explain their varying alkali release and reactivity behaviours, as shown in Table 3.1 and 3.2. For example, woody char contains medium K and Ca with a low Si. Straw contains the highest Si and K. In comparison, IC contains the highest Ca and Mg.

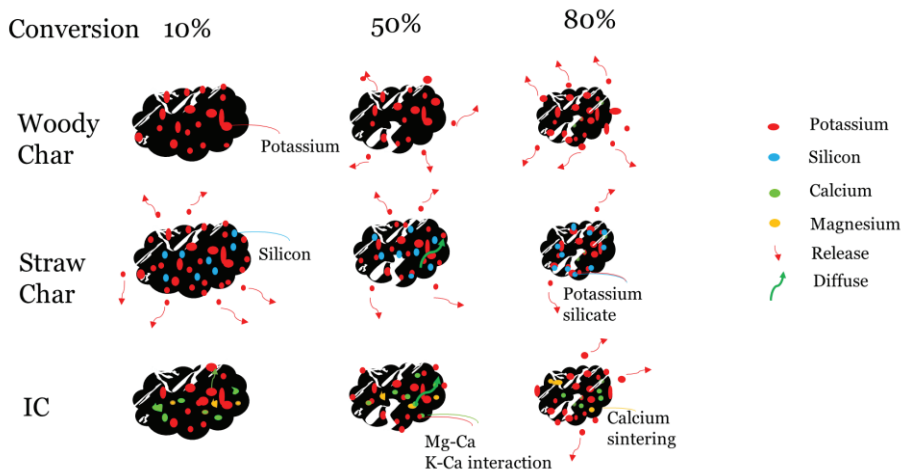

Figure 5.10 Mechanism of alkali release process during biochar gasification process.

The proposed mechanism for woody char alkali release is shown at the top of Figure 5.10. The K content gradually decreases until 80% converted, followed by an increase in K release. With the consumption of the char, more of the K distributed inside the char particle approaches the pore entrance, which improves agent access to the K. The migration of alkali happens from the internal carbon matrix structure to the gas–solid interface. Bulk alkali can dissociate to form intermediates, while calcium can bond with two sites in the char and connects more strongly to biochar than K does [147]. The final peak in alkali release observed for woody chars (Figure 5.1b and 5.8b) is likely related to an increase in the instantaneous char reaction rate. As the K/C ratio increases, more active sites are formed, leading to a significant catalytic effect of alkali. Additionally, free alkali not bound to the char matrix are also present, contributing to the observed release of alkali. In general, the results depicted in Figure 5.9 indicate that K diffuses from the inner particle to the surface

and bulk (route 1), with some being released (route 5), and the rest bonding with the newly formed edge site (route 6), resulting in an increase in *R*.

The ash content from straw char had a very different composition, dominated by Si, followed by K and Ca. As a result, straw char displays a different gasification mechanism (Figure 5.10). There is large potassium release at the beginning of the gasification stage, which gradually decreases (Figure 5.1d and 5.8b), but *R* seems to remain low throughout process (Figure 5.1e and 5.8c). This is because the K was already saturated on the straw char particles at the beginning of the process, and there are no free functional groups available to capture excess K. Moreover, as the conversion proceeds, the relatively high silicon content (Table 3.2) together with potassium forms melted ash that can encapsulate the char [132], so inhibiting the catalytic effects of K and limiting its release. Therefore, the *R* of straw char is always low. As described in Figure 5.9, K diffuses from the inner particles to the surface and bulk (route 1) and keeps releasing due to straw's high potassium content (route 5), while the remainder is bonded with other minerals (route 4), resulting in a low *R*.

The IC sample contains the highest calcium of these three samples and was pre-treated at a high temperature (1200 °C). It does not exhibit any alkali release initially (as seen in Figure 5.5c), possibly because surface alkali has already been released due to the high temperature gasification and the remaining K is captured inside the particle. Additionally, due to the high calcium content, a portion of the alkali interacts with calcium, especially at a temperature of 900 °C [148] which can limit alkali release. At the later stage of the reaction ($X > 70\%$), the release behaviour is the same as for other woody chars because more active sites have been formed and more K is exposed on the surface. This leads to the release due to carbon conversion. As can be observed from Figure 5.9 and 5.10, when conversion is lower than 80%, K mainly diffuses from the inner particle to the surface and bulk (route 1) and combines with Ca (route 4). When the conversion is higher than 80%, K is released due to carbon conversion (route 5).

It is important to note that particle migration is more pronounced in a fixed bed reactor than in a TGA. The TGA uses small char samples with good heat distribution, whereas a fixed bed reactor is a more complex setup that better simulates larger gasifiers. However, the fixed bed reactor presents challenges as heat and gas must travel through tightly packed char particles, resulting in uneven heating and gasification, which may affect gas production rates and species. As shown in Figure 5.11, an ash layer forms at the bottom of the char bed during char conversion. As described in Figure 5.9, volatile alkali from the ash layer can be absorbed to the char surface (route 2) and partially diffuse into the inter-pores of the carbon matrix (route 1), similar to the residual alkali in the char. A part of the alkali(s) from ash or from the gas phase can either contact the gasifying agent to form O* (routes 7 and 8) or bind with oxygen, forming stable oxygen-containing structures, mainly C-O-K

and COO-K structures [149] (route 6). The rest are released from the char bed. Moreover, volatile alkali(s) exhibit better catalytic activity than residual alkali, which may be due to the more stable volatile alkali species and char matrix or the better dispersion effect of volatile alkali [150].

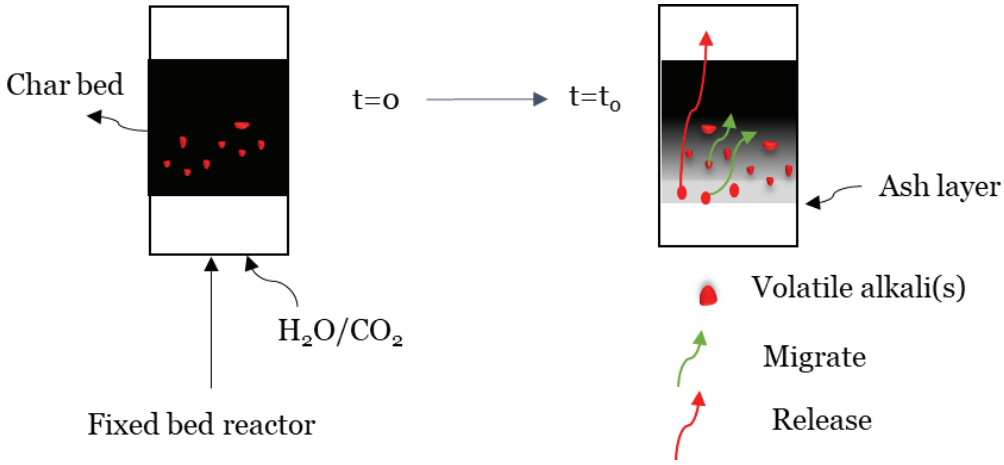

Figure 5.11 Alkali transport behaviour in a fixed bed reactor.

In general, under the same operating conditions, the main difference between CO_2 and steam is that under steam the biochar–H_2O reaction occurs throughout the whole biochar particle, namely the carbon matrix and the gas–solid interface, while under CO_2 conditions the reaction mainly occurs on the gas–char interface [103]. Under steam conditions, water vapour can easily penetrate the porous structure of biochar and react with carbon at various locations within the particle. On the other hand, in CO_2 gasification, CO_2 has lower reactivity with carbon compared to steam, and the reaction rate is slower. CO_2 molecules also have a larger kinetic diameter than H_2O molecules [151], making it difficult for them to penetrate the porous structure of biochar. Moreover, CO_2 is formed during H_2O gasification, making it challenging to conduct a purely H_2O gasification study. The results from steam gasification (Paper IV) align with the findings from CO_2 gasification (Paper III) for all three types of char as regards the impact of conversion on reactivity and alkali release. However, a detailed quantitative comparison of the two studies is difficult due to differences in the experimental setups, sample sizes, and other parameters. Therefore, future research should aim to use consistent experimental procedures to provide a more accurate comparison of the gasification performance of CO_2 and H_2O.

The release and interaction of alkali with char particles and bed materials play a critical role in both heterogeneous and homogeneous reactions during the gasification process. The results from sections 5.2 and 5.3 highlight the behaviors of

alkali metal release in different biochars. Woody char typically releases alkali metals at above 80% conversion (Figure 5.1d and Figure 5.8b), whereas agricultural char tends to release large amounts of alkali metals during the early stages of conversion (Figure 5.8b) and continues to release until the end of char conversion. The alkali release at different stages of conversion ultimately affects gasifier performance. This is particularly the case in regard to fixed bed reactors, where fuel conversion occurs in different zones and the resulting gases flow through the bed before exiting the reactor [45]. In updraft gasifiers, gas-phase alkali released during char oxidation can transfer to the reduction zone and affect the char gasification rate, while in downdraft gasifiers, alkali released from the pyrolysis zone can travel down to the oxidation zone and impact char conversion.

In direct fluidized bed gasifiers, alkali and bed particles interact to create active bed materials that facilitate the gasification of char and catalytic conversion of hydrocarbons within the bed [152, 153]. Alkali is important in this type of gasifier. However, the fact that all conversion processes take place in a single reactor, the released alkali will be uniformly distributed within the bed due to good mixing, of course there is local variations in fuel-bed mixing. As a result, it is challenging to identify any clear benefits of knowing when the alkali is released during the conversion process for these gasifiers.

In dual fluidized bed gasifiers, char is gasified and combusted in separate reactors, with bed material transfer between them to provide the heat needed for the gasification process. The location of alkali release during char conversion inside the gasifier depends on the ash content of the biomass. For example, high ash content biomass, such as straw, results in most of the alkali release occurring in the gasification zone, while for low-ash content char a larger proportion of release occurr in the combustion chamber. This has a significant impact on the formation of active bed material, which is crucial for efficient char and catalytic hydrocarbon conversion [153], as well as gas-phase tar reforming where alkali acts as a catalyst in homogeneous reactions within the gasifier reactor. The importance of alkali has also been emphasized by Furusjö et al. [154] in entrained flow gasifiers. They have shown that adding 2–8% alkali catalyst to the gasification process can transform the slag phase into an alkali carbonate melt, resulting in improved flexibility and up to 90% sulphur capture. This simplifies the process of gas purification required for biofuel production.

Chapter 6

Release of alkali during co-gasification

Co-gasification is a method for efficiently converting fuels through thermal conversion [155,156]. Synergistic effects in this process result from migration of alkali from an alkali-rich fuel to an alkali-deficient fuel. Previous studies have often used a single alkali-rich biomass to enhance coal gasification [29–31]. As discussed in the previous chapter, wood and straw have distinct alkali release profiles during char gasification. Thus, it is of interest to study the levels of alkali release when wood and straw are mixed.

This chapter reports on research from co-gasification of wood and straw mixtures in paper V.

6.1 Synergistic effects and alkali migration during co-gasification

In order to evaluate the potential synergistic effects of combining wood and straw in the mixtures, theoretical reactivity and alkali release rates were calculated using Equation (3-4), which linearly combines results from pure wood and pure straw cases. The experimental and calculated rates are shown in Figure 6.1. All forms of interaction between the straw char and woody char during co-gasification is neglected for the calculated rates.

Figure 6.1a indicates that the co-gasification process of the mixtures is faster experimentally than the theoretically predicted outcomes, implying synergistic effects in the conversion. To evaluate the synergistic effect at different conversion stages, a synergy index (*SI*) was calculated (Equation 3-5) and used (Figure 6.1b). Several factors can affect synergy, including the type of biochar, the blending ratio, the gasification temperature and reactor, and the biochar pre-treatment methods [156]. The results show that the mixing ratio WS75 (75% wood and 25% straw) has the highest *SI*, suggesting that this ratio provides the strongest synergistic effect.

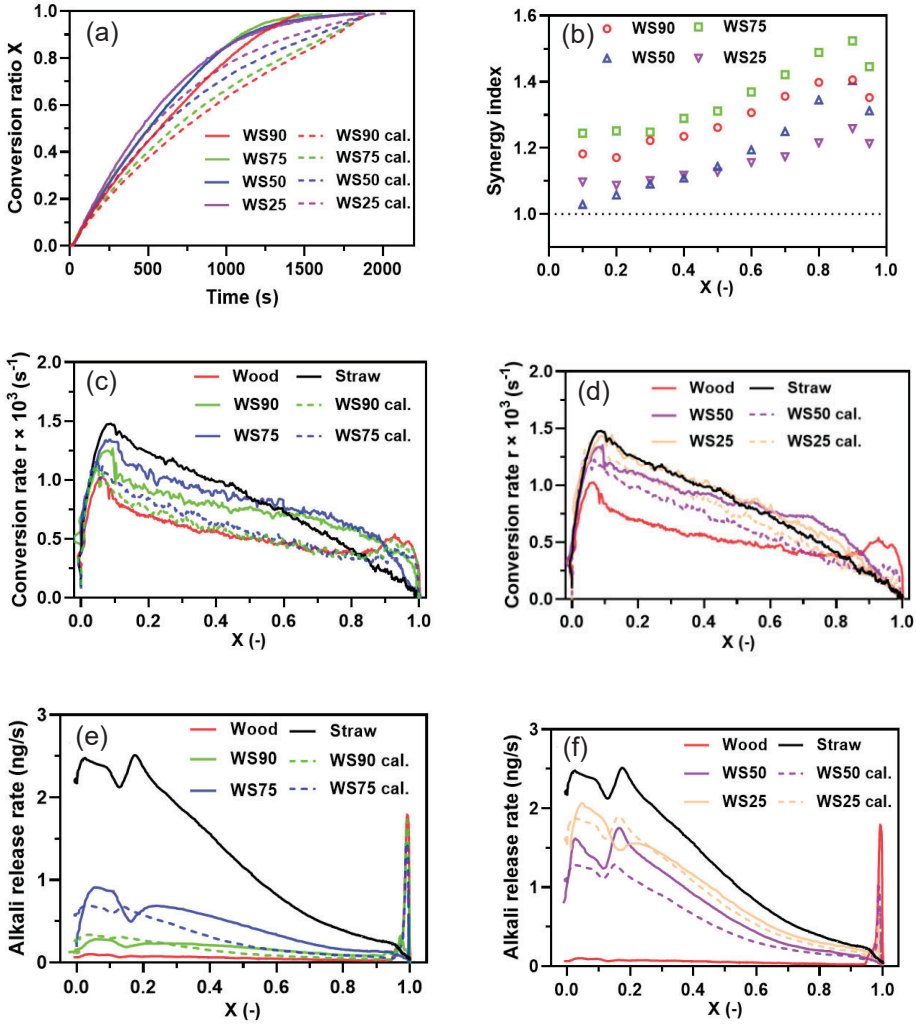

Figure 6.1 Co-gasification of different mixed materials at 900 °C: (a) time versus experimental and calculated conversion ratio *X*; (b) synergy index (*SI*) as a function of *X*; (c) experimental and calculated conversion rate *r* of the mixture and (e) alkali release rate as a function of *X* with mixing ratios of 90:10 and 75:25; (d) conversion rate *r* of the mixture; (f) alkali release rate as a function of *X* with mixing ratios of 50:50 and 25:75.

The conversion rate as a function of conversion X during co-gasification is shown in Figure 6.1c and d for various blend ratios. The experimental conversion rates are higher than the calculated rates for the same conversion across most of the gasification stages. This is due to alkali migration from the straw surface to the wood surface [30]. For all mixing ratios (Figure 6.1e and 6.1f), the experimental alkali release is higher than the calculated amount when the conversion is lower than 90%,

indicating that alkali has migrated from the straw to the wood. This migration most likely occurs when alkali desorbed from straw to the gas phase between particles adsorbs on the woody char surface, which has a large surface area and low alkali content, or through the transfer of low-melting-point alkali melts in contact between particles [157,158]. The implied alkali migration taking place in the mixtures is further confirmed by SEM-EDS results, as described in Paper V. For mixtures with a wood content of 90%, the alkali release in the final stage of pure wood gasification disappears. This may be attributed to migration of Si, Al, and P that react with the alkali to form catalytically inactive compounds [31,144,159–161].

6.2 Effect of temperature during co-gasification

Figure 6.2 illustrates the experimental and calculated co-gasification of WS90 at different temperatures. The largest *SI* is observed at a temperature of 900 °C (Figure 6.2b), which is consistent with the result of co-gasification of biochar and coal [162,163].

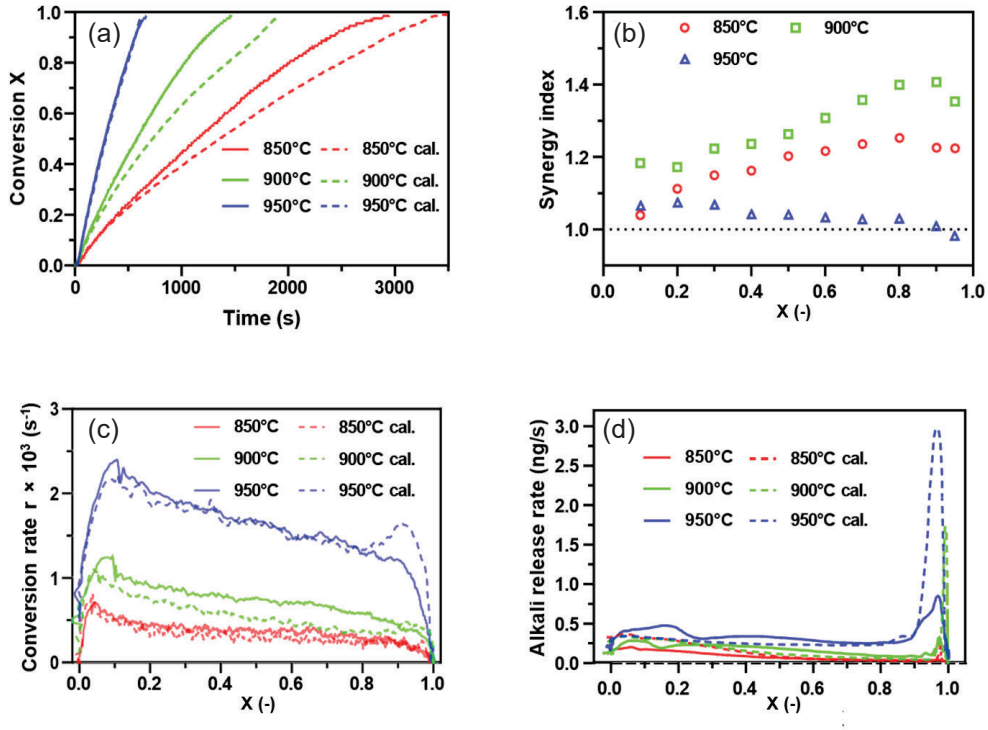

Figure 6.2 Experimental and calculated co-gasification of WS90 at 850 °C, 900 °C, and 950 °C (a) char conversion ratio *X* versus time; (b) synergy index variation for different conversion ratios; (c) conversion rate *r* versus *X*; (d) alkali release rate versus *X*.

Ren et al. [162] found that the synergistic effect of coal char and food char blends was highest at 850–900 °C and decreased at higher temperatures (900–1000 °C). At a lower temperature (850 °C), it is more difficult for the AAEMs in straw char to transfer uniformly to the wood char surface due to lower mobility [156], which limits the catalytic effects.

At 950 °C the difference between experimental and calculated data became smaller as the carbon conversion increased (Figure 6.2c) and showed the lowest *SI* effect (Figure 6.2b), indicating a decrease in the catalytic activity. There are three possible explanations for this: 1) At high temperatures, the reaction rate is limited by the transport of reactants to the reaction site rather than the reaction kinetics, leading to a shift to diffusion-controlled behaviour [164]. 2) The reactions between alkali species, SiO_2, and Al_2O_3 are enhanced [32,165–167], and the gas phase alkali adsorption capacity of wood char is decreased [168,169]. The decrease in adsorption capacity reduces the overall catalytic effect of the system. 3) Calcium also rapidly deactivates by sintering or agglomeration at the high gasification temperatures [170]. All of these options reduce the active alkali content on the sample surface and weaken the catalytic effect, making the overall rate enhancement marginal at 950 °C.

Chapter 7
Conclusions

This thesis presents the findings of studies on the relationship between char reactivity and the development of pore structure, as well as the effects of alkalis and alkali release during char gasification. A reliable method was established to measure alkali release and sample mass simultaneously during char thermal conversion by integrating a surface ionization detector (SID) with a commercial thermogravimetric analyser (TGA) for online alkali measurements. A laboratory-scale reactor system was also used, consisting of diluters, a CO/CO_2 analyser, a scan mobility particle sizer, an optical particle sizer, and a SID.

The impact of porous structure development and alkali on the steam gasification reactivity of biochar was studied first. The findings indicated that gasification temperature had a minimal impact on porous structure development, while the total surface area of the char increased three-fold, and the total pore volume increased between 2.0 to 5.3 times at all temperatures. The micropore generation is proportional to the observed reactivity, particularly at conversions up to 70%. As the conversion process progressed beyond 70%, the catalytic effects of potassium in the char became more prominent.

The potassium-induced phenomena investigated for char samples with similar structures but varying intrinsic potassium content revealed that all samples exhibited a common critical potassium surface coverage (K/C ratio). At this point the catalytic effects became dominant, regardless of temperature or initial potassium content. The modified random pore model accurately described the later stages of conversion by incorporating two additional parameters (c and p). The c constant is related to the intrinsic potassium content and is temperature-independent, while a clear correlation between potassium content and the p parameter was observed with an underlying temperature dependence.

Using TGA-SID to measure real-time alkali release during CO_2 gasification of different types of biochar showed significant differences between woody char and straw char. Alkali release from woody char remained low and constant during most of the process, then increased significantly at the final stage. This suggests that alkali was enriched during the process prior to final release. By contrast, alkali release from straw char decreased continuously during gasification, corresponding to carbon conversion. High temperature and CO_2 concentration promoted char gasification and increased alkali release.

Alkali release during steam gasification of chars was studied in a fixed bed reactor. A small char particle size (125 μm) enhances alkali release at all conversion stages and increases reactivity compared to larger char particles (235 μm), particularly in the early stage of the process. Industrial char and furniture waste char released significant amounts of alkali when char conversion was near completion, similar to the observation for CO_2 gasification. Alkali release from straw char decreased throughout the gasification process. These findings are essential for predicting the performance of industrial-scale gasifiers, particularly in the case of fixed bed reactors.

Finally, the co-gasification of wood and straw showed an apparent synergistic effect on fuel conversion and alkali release. Co-gasification of the two materials significantly improved reactivity when the wood content was relatively high (75%) at 900 °C. SEM-EDS analysis indicated that silicon from straw migrated to the wood surface, reacting with alkali, and inhibiting char reactivity and alkali release during the final stage ($X > 90\%$) of gasification.

This thesis provides new insights into char structure development, alkali release, and element migration during biochar gasification under CO_2 and steam conditions. The findings have valuable implications for industrial processes, especially in relation to alkali release during gasification and co-gasification of fuels. Further study is required to assess the impact of other minerals, including alkaline earth metals, to create a comprehensive kinetic model for char conversion and alkali release during gasification. In addition, it would be useful to develop new techniques for online alkali measurement, particularly to distinguish between potassium and sodium. Additional analysis may also involve studying the active catalytic sites or alkali structure using other methods such as CO_2-chemisorption or X-ray diffraction. Furthermore, future research should aim to compare the mechanisms of CO_2 and steam char gasification.

Acknowledgements

The Swedish Energy Agency is acknowledged for funding this project.

I would like to express my gratitude to my main supervisor, Professor Klas Engvall, for his constant support and guidance throughout my research. Your patience and encouragement have been invaluable to me, and your expertise and advice will be beneficial to me for the rest of my life. I am grateful to have had you not only as a supervisor but also as a mentor and role model.

I also want to thank my co-supervisor, Associate Professor Efthymios Kantarelis, for his invaluable suggestions and support in the lab, which contributed to the successful outcome of this work. Additionally, I am grateful for the valuable conversations we had outside of research, which provided me with fresh perspectives and opportunities for growth.

I am also grateful to my colleagues at the University of Gothenburg, Professor Jan Pettersson for your guidance and discussions, Dr Xiangrui Kong for our valuable conversations, and Yaxin Ge for conducting experiments together and supporting each other.

Thanks to all my colleagues and friends at Chemical Engineering Department. Many thanks to Christer, Lars, Henrik, Lea, Elise, Steven, Kasra, Ali, Alagar, Sandra, Jonas, Zari, Jacob, Pol, Nima, Kai, Aijuan, Yohannes and Dan. Working with you has been an unforgettable experience. All the lovely activities, fikas, Christmas parties, crayfish parties and movie nights are now unforgettable memories that I cherish deeply.

Many thanks to all my friends. My special thanks go to Xinyi, Yuren, Shuang, Fangyuan, Ruoqi, Meng, Han, Yang, Merve, Hong, Tong, Ran and Teng, who helped me a lot and gave me your love, care and shelter when I experienced ups and downs.

I am grateful to my two furry companions, Huahua and Nysko, for their cuddles that bring joy and comfort to my life.

I want to express my deep appreciation to my dear parents-in-law Judit and Hans, and my sister-in-law Siri for treating me like a part of their family and showering me with love and kindness.

To my dearest son Lambert (乐允), you have brought so much joy, love, and strength into my life. You are a constant source of support and encouragement, and I am grateful to have you by my side. 妈妈永远爱你。

I would like to express my deepest gratitude to my loving husband, Jens F. Isaksson. Your unwavering love and support mean the world to me, and I know that I can always count on you.

Lastly, I want to thank my parents, Ding Huaihua and Jiangli, and my grandparents for their unwavering love and support. Their endless encouragement has been invaluable to me, and I could never thank them enough. 谢谢你们，我爱你们。

Saiman Ding

Stockholm, April 2023

References

[1] Government Offices of Sweden Ministry of the Environment and Energy, The Swedish Climate Policy Framework 2018.

[2] Acharya B, Dutta A, Basu P. An investigation into steam gasification of biomass for hydrogen enriched gas production in presence of CaO. International Journal of Hydrogen Energy 2010;35(4):1582–9. https://doi.org/10.1016/j.ijhydene.2009.11.109.

[3] Rauch R, Hrbek J, Hofbauer H. Biomass gasification for synthesis gas production and applications of the syngas. WIREs Energy and Environment 2014;3(4):343–62. https://doi.org/10.1002/wene.97.

[4] Ahmed II, Gupta AK. Kinetics of woodchips char gasification with steam and carbon dioxide. Applied Energy 2011;88(5):1613–9. https://doi.org/10.1016/j.apenergy.2010.11.007.

[5] Ding S, Kantarelis E, Engvall K. Effects of porous structure development and ash on the steam gasification reactivity of biochar residues from a commercial gasifier at different temperatures. Energies 2020;13(19):5004. https://doi.org/10.3390/en13195004.

[6] Lin S, Ding L, Zhou Z, Yu G. Discrete model for simulation of char particle gasification with structure evolution. Fuel 2016;186:656–64. https://doi.org/10.1016/j.fuel.2016.09.011.

[7] Avila C, Pang CH, Wu T, Lester E. Morphology and reactivity characteristics of char biomass particles. Bioresource Technology 2011;102:5237–43. https://doi.org/10.1016/j.biortech.2011.01.071.

[8] Bai Y, Lv P, Yang X, Gao M, Zhu S, Yan L et al. Gasification of coal char in H2O/CO2 atmospheres: Evolution of surface morphology and pore structure. Fuel 2018;218:236–46. https://doi.org/10.1016/j.fuel.2017.11.105.

[9] Komarova E, Guhl S, Meyer B. Brown coal char CO_2-gasification kinetics with respect to the char structure. Part I: Char structure development. Fuel 2015;152:38–47. https://doi.org/10.1016/j.fuel.2015.01.107.

[10] Bai Y, Wang Y, Zhu S, Li F, Xie K. Structural features and gasification reactivity of coal chars formed in Ar and CO_2 atmospheres at elevated pressures. Energy 2014;74:464–70. https://doi.org/10.1016/j.energy.2014.07.012.

[11] Mermoud F, Salvador S, Van de Steene L. Influence of the pyrolysis heating rate on the steam gasification rate of large wood char particles. Fuel 2006;85(10-11):1473–82. https://doi.org/10.1016/j.fuel.2005.12.004.

[12] Fu P, Hu S, Xiang J, Sun L, Su S, Wang J. Evaluation of the porous structure development of chars from pyrolysis of rice straw: Effects of pyrolysis temperature and heating rate. Journal of Analytical and Applied Pyrolysis 2012;98:177–83. https://doi.org/10.1016/j.jaap.2012.08.005.

[13] Davidsson KO, Korsgren JG, Pettersson J, Jäglid U. The effects of fuel washing techniques on alkali release from biomass. Fuel 2002;81(2):137–42. https://doi.org/10.1016/S0016-2361(01)00132-6.
[14] Di Blasi C, Branca C, D'Errico G. Degradation characteristics of straw and washed straw. Thermochimica Acta 2000;364(1-2):133–42. https://doi.org/10.1016/S0040-6031(00)00634-1.
[15] Jenkins BM, Bakker RR, Wei JB. On the properties of washed straw. Biomass and Bioenergy 1996;10(4):177–200. https://doi.org/10.1016/0961-9534(95)00058-5.
[16] Zolin A, Jensen A, Jensen PA, Frandsen F, Dam-Johansen K. The influence of inorganic materials on the thermal deactivation of fuel chars. Energy Fuels 2001;15(5):1110–22. https://doi.org/10.1021/ef000288d.
[17] Huang Y, Yin X, Wu C, Wang C, Xie J, Zhou Z et al. Effects of metal catalysts on CO2 gasification reactivity of biomass char. Biotechnology Advances 2009;27(5):568–72. https://doi.org/10.1016/j.biotechadv.2009.04.013.
[18] Karlström O, Dirbeba MJ, Costa M, Brink A, Hupa M. Influence of K/C ratio on gasification rate of biomass chars. Energy & Fuels 2018;32(10):10695–700. https://doi.org/10.1021/acs.energyfuels.8b02288.
[19] Perander M, DeMartini N, Brink A, Kramb J, Karlström O, Hemming J et al. Catalytic effect of Ca and K on CO_2 gasification of spruce wood char. Fuel 2015;150:464–72. https://doi.org/10.1016/j.fuel.2015.02.062.
[20] Suzuki T, Nakajima H, Ikenaga N, Oda H, Miyake T. Effect of mineral matters in biomass on the gasification rate of their chars. Biomass Conversion and Biorefinery 2011;1(1):17–28. https://doi.org/10.1007/s13399-011-0006-2.
[21] Bouraoui Z, Dupont C, Jeguirim M, Limousy L, Gadiou R. CO_2 gasification of woody biomass chars: The influence of K and Si on char reactivity. Comptes Rendus Chimie 2016;19(4):457–65. https://doi.org/10.1016/j.crci.2015.08.012.
[22] Aho A, DeMartini N, Pranovich A, Krogell J, Kumar N, Eränen K et al. Pyrolysis of pine and gasification of pine chars: Influence of organically bound metals. Bioresource Technology 2013;128:22–9. https://doi.org/10.1016/j.biortech.2012.10.093.
[23] Keown DM, Hayashi J, Li C-Z. Drastic changes in biomass char structure and reactivity upon contact with steam. Fuel 2008;87(7):1127–1132. https://doi.org/10.1016/j.biortech.2012.03.072.
[24] Long J, Song H, Jun X, Sheng S, Lun-Shi S, Kai X et al. Release characteristics of alkali and alkaline earth metallic species during biomass pyrolysis and steam gasification process. Bioresource Technology 2012;116:278–84. https://doi.org/10.1016/j.biortech.2012.03.051.
[25] Wang C, Wu Y, Liu Q, Yang H, Wang F. Analysis of the behaviour of pollutant gas emissions during wheat straw/coal cofiring by TG–FTIR. Fuel Processing

Technology 2011;92(5):1037–41. https://doi.org/10.1016/j.fuproc.2010.12.029.
[26] Agbor E, Zhang X, Kumar A. A review of biomass co-firing in North America. Renewable and Sustainable Energy Reviews 2014;40:930–43. https://doi.org/10.1016/j.rser.2014.07.195.
[27] Sahu SG, Chakraborty N, Sarkar P. Coal–biomass co-combustion: An overview. Renewable and Sustainable Energy Reviews 2014;39:575–86. https://doi.org/10.1016/j.rser.2014.07.106.
[28] Sami M, Annamalai K, Wooldridge M. Co-firing of coal and biomass fuel blends. Progress in Energy and Combustion Science 2001;27(2):171–214. https://doi.org/10.1016/S0360-1285(00)00020-4.
[29] Wei J, Song X, Guo Q, Ding L, Yoshikawa K, Yu G. Reactivity, synergy, and kinetics analysis of CO2 co-pyrolysis/co-gasification of biomass after hydrothermal treatment and coal blends. Energy & Fuels 2020;34(1):294–303. https://doi.org/10.1021/acs.energyfuels.9b03721.
[30] Lahijani P, Zainal ZA, Mohamed AR, Mohammadi M. Co-gasification of tire and biomass for enhancement of tire-char reactivity in CO_2 gasification process. Bioresource Technology 2013;138:124–30. https://doi.org/10.1016/j.biortech.2013.03.179.
[31] Wei J, Gong Y, Guo Q, Chen X, Ding L, Yu G. A mechanism investigation of synergy behaviour variations during blended char co-gasification of biomass and different rank coals. Renewable Energy 2019;131:597–605. https://doi.org/10.1016/j.renene.2018.07.075.
[32] Zhang Y, Zheng Y, Yang M, Song Y. Effect of fuel origin on synergy during co-gasification of biomass and coal in CO_2. Bioresource Technology 2016;200:789–94. https://doi.org/10.1016/j.biortech.2015.10.076.
[33] The Sustainable Development Goals Report 2022; Available from: https://unstats.un.org/sdgs/report/2022/.
[34] Willis K. The Sustainable Development Goals. In: Cupples J, Palomino-Schalscha M, Prieto M (eds), The Routledge Handbook of Latin American Development. London: Routledge, 2018, p. 121–131. https://doi.org/10.4324/9781315162935.
[35] Di Blasi C. Combustion and gasification rates of lignocellulosic chars. Progress in Energy and Combustion Science 2009;35(2):121–40. https://doi.org/10.1016/j.pecs.2008.08.001.
[36] Zhang Y, Wan L, Guan J, Xiong Q, Zhang S, Jin X. A review on biomass gasification: effect of main parameters on char generation and reaction. Energy Fuels 2020;34(11):13438–55. https://doi.org/10.1021/acs.energyfuels.0c02900.
[37] Antonio Molino, Simeone Chianese, Dino Musmarra. Biomass gasification technology: The state of the art overview. Journal of Energy Chemistry 2016;25(1):10–25. https://doi.org/10.1016/j.jechem.2015.11.005.

[38] Sansaniwal SK, Pal K, Rosen MA, Tyagi SK. Recent advances in the development of biomass gasification technology: A comprehensive review. Renewable and Sustainable Energy Reviews 2017;72:363–84. https://doi.org/10.1016/j.rser.2017.01.038.
[39] Kumar A, Eskridge K, Jones DD, Hanna MA. Steam-air fluidized bed gasification of distillers grains: Effects of steam to biomass ratio, equivalence ratio and gasification temperature. Bioresource Technology 2009;100(6):2062–8. https://doi.org/10.1016/j.biortech.2008.10.011.
[40] Widyawati M, Church TL, Florin NH, Harris AT. Hydrogen synthesis from biomass pyrolysis with in situ carbon dioxide capture using calcium oxide. International Journal of Hydrogen Energy 2011;36(8):4800–13. https://doi.org/10.1016/j.ijhydene.2010.11.103.
[41] Milne TA, Evans RJ, Abatzaglou N. Biomass Gasifier "Tars": Their Nature, Formation, and Conversion; 1998, NREL/TP-570-25357. https://doi.org/2172/3726.
[42] Moersch O, Spliethoff H, Hein K. Tar quantification with a new online analyzing method. Biomass and Bioenergy 2000;18(1):79–86. https://doi.org/10.1016/S0961-9534(99)00068-9.
[43] Douglas C. Elliott. Relation of reaction time and temperature to chemical composition of pyrolysis oils. In: Pyrolysis Oils From Biomass.
[44] Xu C, Donald J, Byambajav E, Ohtsuka Y. Recent advances in catalysts for hot-gas removal of tar and NH3 from biomass gasification. Fuel 2010;89(8):1784–95. https://doi.org/10.1016/j.fuel.2010.02.014.
[45] Basu P. Pyrolysis and Torrefaction: Practical Design and Theory. Academic press; 2018.
[46] Mishra A, Gautam S, Sharma T. Effect of operating parameters on coal gasification. International Journal of Coal Science & Technology 2018;5(2):113–25. https://doi.org/10.1007/s40789-018-0196-3.
[47] Vigouroux RZ. Pyrolysis of biomass. Dissertation KTH, Stockholm, 2021.
[48] Mishra S, Upadhyay RK. Review on biomass gasification: Gasifiers, gasifying mediums, and operational parameters. Materials Science for Energy Technologies 2021;4:329–40. https://doi.org/10.1016/j.mset.2021.08.009.
[49] Ren J, Cao J-P, Zhao X-Y, Yang F-L, Wei X-Y. Recent advances in syngas production from biomass catalytic gasification: A critical review on reactors, catalysts, catalytic mechanisms and mathematical models. Renewable and Sustainable Energy Reviews 2019;116:109426. https://doi.org/10.1016/j.rser.2019.109426.
[50] Molino A, Larocca V, Chianese S, Musmarra D. Biofuels production by biomass gasification: A review. Energies 2018;11(4):811. https://doi.org/10.3390/en11040811.

[51] Di Blasi C, Signorelli G, Di Russo C, Rea G. Product distribution from pyrolysis of wood and agricultural residues. Industrial & Engineering Chemistry Research 1999;38(6):2216–24. https://doi.org/10.1021/ie980711u.
[52] Lv D, Xu M, Liu X, Zhan Z, Li Z, Yao H. Effect of cellulose, lignin, alkali and alkaline earth metallic species on biomass pyrolysis and gasification. Fuel Processing Technology 2010;91(8):903–9. https://doi.org/10.1016/j.fuproc.2009.09.014.
[53] Sikarwar VS, Zhao M, Clough P, Yao J, Zhong X, Memon MZ et al. An overview of advances in biomass gasification. Energy & Environmental Science 2016;9(10):2939–77. https://doi.org/10.1039/C6EE00935B.
[54] Shen Y, Linville JL, Ignacio-de Leon PAA, Schoene RP, Urgun-Demirtas M. Towards a sustainable paradigm of waste-to-energy process: Enhanced anaerobic digestion of sludge with woody biochar. Journal of Cleaner Production 2016;135:1054–64. https://doi.org/10.1016/j.jclepro.2016.06.144.
[55] You S, Ok YS, Chen SS, Tsang DCW, Kwon EE, Lee J et al. A critical review on sustainable biochar system through gasification: Energy and environmental applications. Bioresource Technology 2017;246:242–53. https://doi.org/10.1016/j.biortech.2017.06.177.
[56] Bridgwater AV. Review of fast pyrolysis of biomass and product upgrading. Biomass and Bioenergy 2012;38:68–94. https://doi.org/10.1016/j.biombioe.2011.01.048.
[57] Radlein D, Quignard A. A short historical review of fast pyrolysis of biomass. Oil & Gas Science and Technology – Revue d'IFP Energies nouvelles 2013;68(4):765–83. https://doi.org/10.2516/ogst/2013162.
[58] Guizani C, Jeguirim M, Valin S, Limousy L, Salvador S. Biomass Chars: The effects of pyrolysis conditions on their morphology, structure, chemical properties and reactivity. Energies 2017;10(6):796. https://doi.org/10.3390/en10060796.
[59] Septien S, Escudero Sanz FJ, Salvador S, Valin S. The effect of pyrolysis heating rate on the steam gasification reactivity of char from woodchips. Energy 2018;142:68–78. https://doi.org/10.1016/j.energy.2017.09.114.
[60] Senneca O. Kinetics of pyrolysis, combustion and gasification of three biomass fuels. Fuel Processing Technology 2007;88(1):87–97. https://doi.org/10.1016/j.fuproc.2006.09.002.
[61] Gil MV, Riaza J, Álvarez L, Pevida C, Rubiera F. Biomass devolatilization at high temperature under N_2 and CO_2: Char morphology and reactivity. Energy 2015;91:655–62. https://doi.org/10.1016/j.energy.2015.08.074.
[62] Bai Y, Wang Y, Zhu S, Li F, Xie K. Structural features and gasification reactivity of coal chars formed in Ar and CO_2 atmospheres at elevated pressures. Energy 2014;74:464–70. https://doi.org/10.1016/j.energy.2014.07.012.

[63] Guizani C, Jeguirim M, Gadiou R, Escudero Sanz FJ, Salvador S. Biomass char gasification by H_2O, CO_2 and their mixture: Evolution of chemical, textural and structural properties of the chars. Energy 2016;112:133–45. https://doi.org/10.1016/j.energy.2016.06.065.
[64] Kajita M, Kimura T, Norinaga K, Li C-Z, Hayashi J. Catalytic and noncatalytic mechanisms in steam gasification of char from the pyrolysis of biomass. Energy & Fuels 2010;24(1):108–16. https://doi.org/10.1021/ef900513a.
[65] Fu P, Hu S, Xiang J, Yi W, Bai X, Sun L et al. Evolution of char structure during steam gasification of the chars produced from rapid pyrolysis of rice husk. Bioresource Technology 2012;114:691–7. https://doi.org/10.1016/j.biortech.2012.03.072.
[66] Wu H, Yip K, Tian F, Xie Z, Li C-Z. Catalytic and noncatalytic mechanisms in steam gasification of char from the pyrolysis of biomass. Industrial & Engineering Chemistry Research 2009;48(23):10431–8. https://doi.org/10.1021/ie901025d.
[67] Zhang Y, Ashizawa M, Kajitani S, Miura K. Proposal of a semi-empirical kinetic model to reconcile with gasification reactivity profiles of biomass chars. Fuel 2008;87(4-5):475–81. https://doi.org/10.1016/j.fuel.2007.04.026.
[68] Nzihou A, Stanmore B, Sharrock P. A review of catalysts for the gasification of biomass char, with some reference to coal. Energy 2013;58:305–17. https://doi.org/10.1016/j.energy.2013.05.057.
[69] Wang J, Jiang M, Yao Y, Zhang Y, Cao J. Steam gasification of coal char catalyzed by K_2CO_3 for enhanced production of hydrogen without formation of methane. Fuel 2009;88(9):1572–9. https://doi.org/10.1016/j.fuel.2008.12.017.
[70] Yip K, Tian F, Hayashi J, Wu H. Effect of alkali and alkaline earth metallic species on biochar reactivity and syngas compositions during steam gasification. Energy & Fuels 2010;24(1):173–81. https://doi.org/10.1021/ef900534n.
[71] Dahou T, Defoort F, Nguyen HN, Bennici S, Jeguirim M, Dupont C. Biomass steam gasification kinetics: relative impact of char physical properties vs. inorganic composition. Biomass Conversion and Biorefinery 2022;12(8):3475–90. https://doi.org/10.1007/s13399-020-00894-9.
[72] Lecea CS-M de, Almela-Alarcón M, Linares-Solano A. Calcium-catalysed carbon gasification in CO2 and steam. Fuel 1990;69(1):21–7. https://doi.org/10.1016/0016-2361(90)90253-M.
[73] Ban Y, Liu Q, Zhou H, Li N, Zhao B, Shi S et al. Catalytic effect of representative calcium salts on the steam gasification of a Shengli lignite. Fuel 2019;255:115832. https://doi.org/10.1016/j.fuel.2019.115832.
[74] Radovic LR, Steczko K, Walker PL, Jenkins RG. Combined effects of inorganic constituents and pyrolysis conditions on the gasification reactivity of coal

chars. Fuel Processing Technology 1985;10(3):311–26. https://doi.org/10.1016/0378-3820(85)90038-4.
[75] Liu F, Yu G, Yu D, Chen S, Han J, Yu X et al. Calcium catalytic behavior during in-situ gasification of different aged coal chars in CO_2 and steam. Fuel 2021;287:119803. https://doi.org/10.1016/j.fuel.2020.119803.
[76] Ohtsuka Y, Asami K. Steam gasification of coals with calcium hydroxide. Energy Fuels 1995;9(6):1038–42. https://doi.org/10.1021/ef00054a016.
[77] Chen Y, Luo Z, Fang M, Wang Q. Migration and transformation of sodium during staged coal combustion of Zhundong coal and influence of carbon coating. Fuel Processing Technology 2020;203:106382. https://doi.org/10.1016/j.fuproc.2020.106382.
[78] Mlonka-Mędrala A, Magdziarz A, Gajek M, Nowińska K, Nowak W. Alkali metals association in biomass and their impact on ash melting behaviour. Fuel 2020;261:116421. https://doi.org/10.1016/j.fuel.2019.116421.
[79] Tang J, Guo R, Wang J. Inhibition of interaction between kaolinite and K_2CO_3 by pretreatment using calcium additive. Journal of Thermal Analysis and Calorimetry 2013;114(1):153–60. https://doi.org/10.1007/s10973-012-2905-2.
[80] Jiang M-Q, Zhou R, Hu J, Wang F-C, Wang J. Calcium-promoted catalytic activity of potassium carbonate for steam gasification of coal char: Influences of calcium species. Fuel 2012;99:64–71. https://doi.org/10.1016/j.fuel.2012.04.007.
[81] Arnold RA, Habibi R, Kopyscinski J, Hill JM. Interaction of Potassium and Calcium in the Catalytic Gasification of Biosolids and Switchgrass. Energy Fuels 2017;31(6):6240–7. https://doi.org/10.1021/acs.energyfuels.7b00972.
[82] Ramsurn H, Kumar S, Gupta RB. Enhancement of biochar gasification in alkali hydrothermal medium by passivation of inorganic components using Ca(OH)2. Energy & Fuels 2011;25(5):2389–98. https://doi.org/10.1021/ef200438b.
[83] Liu L, Liu H, Cui M, Hu Y, Wang J. Calcium-promoted catalytic activity of potassium carbonate for steam gasification of coal char: Transformations of sulfur. Fuel 2013;112:687–94. https://doi.org/10.1016/j.fuel.2012.06.048.
[84] Xu J, Wang J, Du C, Li S, Liu X. Understanding fusibility characteristics and flow properties of the biomass and biomass-coal ash samples. Renewable Energy 2020;147:1352–7. https://doi.org/10.1016/j.renene.2019.09.066.
[85] Guo Q, Cheng Z, Chen G, Yan B, Li J, Hou L et al. Assessment of biomass demineralization on gasification: From experimental investigation, mechanism to potential application. Science of the Total Environment 2020;726:138634. https://doi.org/10.1016/j.scitotenv.2020.138634.
[86] Skoulou V, Kantarelis E, Arvelakis S, Yang W, Zabaniotou A. Effect of biomass leaching on H2 production, ash and tar behavior during high temperature

steam gasification (HTSG) process. International Journal of Hydrogen Energy 2009;34(14):5666–73. https://doi.org/10.1016/j.ijhydene.2009.05.117.
[87] Yoo H-M, Park S-W, Jeong Y-O, Han G-H, Choi HS, Seo Y-C. Enhancement of gasification performance for palm oil byproduct by removal of alkali and alkaline earth metallic compounds and ash. Energy Fuels 2019;33(6):5263–9. https://doi.org/10.1021/acs.energyfuels.9b00158.
[88] Zhang Y, Ashizawa M, Kajitani S. Calcium loading during the dewatering of wet biomass in kerosene and catalytic activity for subsequent char gasification. Fuel 2008;87(13-14):3024–30. https://doi.org/10.1016/j.fuel.2008.03.009.
[89] Du Y, Zhao N, Wang J, Zhang J, Wang C, Che D. Effect of CO2 on coal devolatilization in oxy-fuel combustion: Exploring the influence of temperature and inherent alkali/alkaline earth metal. International Journal of Greenhouse Gas Control 2020;96:103004. https://doi.org/10.1016/j.ijggc.2020.103004.
[90] Link S, Arvelakis S, Hupa M, Yrjas P, Külaots I, Paist A. Reactivity of the biomass chars originating from reed, Douglas fir, and pine. Energy & Fuels 2010;24(12):6533–9. https://doi.org/10.1021/ef100926v.
[91] Gusta E, Dalai AK, Uddin MA, Sasaoka E. Catalytic decomposition of biomass tars with dolomites. Energy Fuels 2009;23(4):2264–72. https://doi.org/10.1021/ef8009958.
[92] Lahijani P, Zainal ZA, Mohamed AR, Mohammadi M. CO2 gasification reactivity of biomass char: catalytic influence of alkali, alkaline earth and transition metal salts. Bioresource Technology 2013;144:288–95. https://doi.org/10.1016/j.biortech.2013.06.059.
[93] Mckee D, Spiro C, Kosky P, Lamby E. Eutectic salt catalysts for graphite and coal char gasification. Fuel 1985;64(6):805–9. https://doi.org/10.1016/0016-2361(85)90014-6.
[94] Raheem A, Liu H, Ji G, Zhao M. Gasification of lipid-extracted microalgae biomass promoted by waste eggshell as CaO catalyst. Algal Research 2019;42:101601. https://doi.org/10.1016/j.algal.2019.101601.
[95] Li N, Te G, Liu Q, Ban Y, Wang Y, Zhang X et al. Effect of metal ions on the steam gasification performance of demineralized Shengli lignite char. International Journal of Hydrogen Energy 2016;41(48):22837–45. https://doi.org/10.1016/j.ijhydene.2016.09.018.
[96] Śpiewak K, Czerski G, Porada S. Effect of K, Na and Ca-based catalysts on the steam gasification reactions of coal. Part I: Type and amount of one-component catalysts. Chemical Engineering Science 2021;229:116024. https://doi.org/10.1016/j.ces.2020.116024.
[97] Shahbaz M, Yusup S, Inayat A, Patrick DO, Ammar M, Pratama A. Cleaner production of hydrogen and syngas from catalytic steam palm kernel shell gasification using CaO sorbent and coal bottom ash as a catalyst. Energy &

Fuels 2017;31(12):13824–33. https://doi.org/10.1021/acs.energyfuels.7b03237.
[98] Muangrat R, Onwudili JA, Williams PT. Influence of alkali catalysts on the production of hydrogen-rich gas from the hydrothermal gasification of food processing waste. Applied Catalysis B: Environmental 2010;100(3-4):440–9. https://doi.org/10.1016/j.apcatb.2010.08.019.
[99] Chen SG, Yang RT. Unified mechanism of alkali and alkaline earth catalyzed gasification reactions of carbon by CO2 and H2O. Energy & Fuels 1997;11(2):421–7. https://doi.org/10.1021/ef9600990.
[100] McKee DW. Mechanisms of the alkali metal catalysed gasification of carbon. Fuel 1983;62(2):170–5. https://doi.org/10.1016/0016-2361(83)90192-8.
[101]McKee DW. Gasification of graphite in carbon dioxide and water vapor—the catalytic effects of alkali metal salts. Carbon 1982;20(1):59–66. https://doi.org/10.1016/0008-6223(82)90075-6.
[102] Romero Millán LM, Sierra Vargas FE, Nzihou A. Unraveled mechanisms in energy production from bioresources using steam gasification. Fuel 2021;287:119527. https://doi.org/10.1016/j.fuel.2020.119527.
[103] Feng D, Zhao Y, Zhang Y, Xu H, Zhang L, Sun S. Catalytic mechanism of ion-exchanging alkali and alkaline earth metallic species on biochar reactivity during CO_2/H_2O gasification. Fuel 2018;212:523–32. https://doi.org/10.1016/j.fuel.2017.10.045.
[104] Wang J, Yao Y, Cao J, Jiang M. Enhanced catalysis of K2CO3 for steam gasification of coal char by using Ca(OH)2 in char preparation. Fuel 2010;89(2):310–7. https://doi.org/10.1016/j.fuel.2009.09.001.
[105] Mei Y, Wang Z, Zhang S, Fang Y. Novel assumption about the mechanism of catalytic gasification: On the basis of the same catalytic effect of alkali between C–CO2 and Fe–CO2 reactions. Energy & Fuels 2021;35(19):16258–63. https://doi.org/10.1021/acs.energyfuels.1c02159.
[106] Hofbauer H, Materazzi M. Waste gasification processes for SNG production. In: Materazzi M, Foscolo PG (eds). Substitute Natural Gas from Waste. Academic Press, p. 105–160.
[107] Mohammadi A, Anukam A. The technical challenges of the gasification technologies currently in use and ways of optimizing them: A review. In: Vizureanu P, editor. Latest Research on Energy Recovery. IntechOpen; 2023, https://doi.org/10.5772/intechopen.102593.
[108] Sikarwar VS, Zhao M, Fennell PS, Shah N, Anthony EJ. Progress in biofuel production from gasification. Progress in Energy and Combustion Science 2017;61:189–248. https://doi.org/10.1016/j.pecs.2017.04.001.
[109] Vamvuka D, Zografos D, Alevizos G. Control methods for mitigating biomass ash-related problems in fluidized beds. Bioresource Technology 2008;99(9):3534–44. https://doi.org/10.1016/j.biortech.2007.07.049.

[110] Engvall K, Kusar H, Sjöström K, Pettersson LJ. Upgrading of raw gas from biomass and waste gasification: Challenges and opportunities. Top Catal 2011;54(13-15):949–59. https://doi.org/10.1007/s11244-011-9714-x.
[111] Unar IN, Wang L, Pathan AG, Mahar RB, Li R, Uqaili MA. Numerical simulations for the coal/oxidant distribution effects between two-stages for multi opposite burners (MOB) gasifier. Energy Conversion and Management 2014;86:670–82. https://doi.org/10.1016/j.enconman.2014.06.028.
[112] Davidsson KO, Stojkova BJ, Pettersson JBC. Alkali emission from birchwood particles during rapid pyrolysis. Energy & Fuels 2002;16(5):1033–9. https://doi.org/10.1021/ef010257y.
[113] Hagström M, Jäglid U, Pettersson JB. Desorption kinetics at atmospheric pressure: alkali interactions with rhodium and steel surfaces. Applied Surface Science 2000;161(1-2):291–9. https://doi.org/10.1016/S0169-4332(00)00315-9.
[114] Korsgren JG, Pettersson JBC. Collision dynamics and decomposition of NaCl nanometer particles on hot platinum surfaces. The Journal of Physical Chemistry B 1999;103(47):10425–32. https://doi.org/10.1021/jp991585q.
[115] M Jaroniec RM. Physical adsorption on heterogeneous solids. Advances in Colloid and Interface Science; 1988.
[116] Sing KSW. Reporting physisorption data for gas/solid systems with special reference to the determination of surface area and porosity (Recommendations 1984). Pure and Applied Chemistry 1985;57(4):603–19. https://doi.org/10.1351/pac198557040603.
[117] Ding L, Gong Y, Wang Y, Wang F, Yu G. Characterisation of the morphological changes and interactions in char, slag and ash during CO_2 gasification of rice straw and lignite. Applied Energy 2017;195:713–24. https://doi.org/10.1016/j.apenergy.2017.03.098.
[118] Lu GQ, Do DD. Comparison of structural models for high-ash char gasification. Carbon 1994;32:247–63. https://doi.org/10.1016/0008-6223(94)90188-0.
[119] Nowicki L, Antecka A, Bedyk T, Stolarek P, Ledakowicz S. The kinetics of gasification of char derived from sewage sludge. J Therm Anal Calorim 2011;104:693–700. https://doi.org/10.1007/s10973-010-1032-1.
[120] Ishida M, Wen CY. Comparison of zone-reaction model and unreacted-core shrinking model in solid-gas reactions: I isothermal analysis. Chemical Engineering Science 1971;26(7):1031–41. https://doi.org/10.1016/0009-2509(71)80017-9.
[121] Szekely J, Evans JW. A structural model for gas—solid reactions with a moving boundary. Chemical Engineering Science, 25(6), 1091-1107. Chemical Engineering Science 1970;25(6):1091–107. https://doi.org/10.1016/0009-2509(70)85053-9.

[122] Bhatia SK, Perlmutter DD. A random pore model for fluid-solid reactions: I. Isothermal, kinetic control. AIChE Journal, 26(3), 379-386. AIChE J. 1980;26:379–86. https://doi.org/10.1002/AIC.690260308.
[123] Fermoso J, Arias B, Pevida C, Plaza MG, Rubiera F, Pis JJ. Kinetic models comparison for steam gasification of different nature fuel chars. J Therm Anal Calorim 2008;91(3):779–86. https://doi.org/10.1007/s10973-007-8623-5.
[124] Kirtania K, Axelsson J, Matsakas L, Christakopoulos P, Umeki K, Furusjö E. Kinetic study of catalytic gasification of wood char impregnated with different alkali salts. Energy 2017;118:1055–65. https://doi.org/10.1016/j.energy.2016.10.134.
[125]Bai Y, Lv P, Yang X, Gao M, Zhu S, Yan L et al. Gasification of coal char in H2O/CO2 atmospheres: Evolution of surface morphology and pore structure. Fuel 2018;218:236–46. https://doi.org/10.1016/j.fuel.2017.11.105.
[126] Dupont C, Jacob S, Marrakchy KO, Hognon C, Grateau M, Labalette F et al. How inorganic elements of biomass influence char steam gasification kinetics. Energy 2016;109:430–5. https://doi.org/10.1016/j.energy.2016.04.094.
[127]Dupont C, Nocquet T, Da Costa JA, Verne-Tournon C. Kinetic modelling of steam gasification of various woody biomass chars: influence of inorganic elements. Bioresource Technology 2011;102(20):9743–8. https://doi.org/10.1016/j.biortech.2011.07.016.
[128] Fatehi H, Bai X-S. Structural evolution of biomass char and its effect on the gasification rate. Applied Energy 2017;185:998–1006. https://doi.org/10.1016/j.apenergy.2015.12.093.
[129] Struis R, Scala C von, Stucki S, Prins R. Gasification reactivity of charcoal with CO_2. Part I: Conversion and structural phenomena. Chemical Engineering Science 2002;57(17):3581–92. https://doi.org/10.1016/S0009-2509(02)00254-3.
[130] Hognon C, Dupont C, Grateau M, Delrue F. Comparison of steam gasification reactivity of algal and lignocellulosic biomass: influence of inorganic elements. Bioresource Technology 2014;164:347–53. https://doi.org/10.1016/j.biortech.2014.04.111.
[131] Marinkovic J, Thunman H, Knutsson P, Seemann M. Characteristics of olivine as a bed material in an indirect biomass gasifier. Chemical Engineering Journal 2015;279:555–66. https://doi.org/10.1016/j.cej.2015.05.061.
[132] Strandberg A, Holmgren P, Wagner DR, Molinder R, Wiinikka H, Umeki K et al. Effects of pyrolysis conditions and ash formation on gasification rates of biomass char. Energy & Fuels 2017;31(6):6507–14. https://doi.org/10.1021/acs.energyfuels.7b00688.
[133] Sams DA, Shadman F. Catalytic effect of potassium on the rate of char-CO_2 gasification. Fuel 1983;62:880–2. https://doi.org/10.1016/0016-2361(83)90153-9.

[134] Halim N, Tajima A, Asano S, Kudo S, Hayashi J. Change in catalytic activity of potassium during CO2 gasification of char. Energy & Fuels 2020;34(1):225–34. https://doi.org/10.1021/acs.energyfuels.9b03630.
[135]Mims CA, Pabst JK. Role of surface salt complexes in alkali-catalysed carbon gasification. Fuel 1983;62:176–9. https://doi.org/10.1016/0016-2361(83)90193-X.
[136] Ge Yu, Dunxi Yu, Fangqi Liu, Xin Yu, Jingkun Han, Jianqun Wu et al. Different catalytic action of ion-exchanged calcium in steam and CO_2 gasification and its effects on the evolution of char structure and reactivity. Fuel 2019;254:115609. https://doi.org/10.1016/j.fuel.2019.06.017.
[137]Zhang Y, Hara S, Kajitani S, Ashizawa M. Modeling of catalytic gasification kinetics of coal char and carbon. Fuel 2010;89:152–7. https://doi.org/10.1016/j.fuel.2009.06.004.
[138] Dahou T, Defoort F, Jeguirim M, Dupont C. Towards understanding the role of K during biomass steam gasification. Fuel 2020;282:118806. https://doi.org/10.1016/j.fuel.2020.118806.
[139] Dayton DC, French RJ, Milne TA. Direct observation of alkali vapor release during biomass combustion and gasification. 1. Application of molecular beam/mass spectrometry to switchgrass combustion. Energy & Fuels 1995;9(5):855–65. https://doi.org/10.1021/ef00053a018.
[140] Defoort F, Dupont C, Durruty J, Guillaudeau J, Bedel L, Ravel S et al. Thermodynamic study of the alkali release behavior during steam gasification of several biomasses. Energy & Fuels 2015;29(11):7242–53. https://doi.org/10.1021/acs.energyfuels.5b01755.
[141]Mermoud F, Golfier F, Salvador S, van de Steene L, Dirion JL. Experimental and numerical study of steam gasification of a single charcoal particle. Combustion and Flame 2006;145(1-2):59–79. https://doi.org/10.1016/j.combustflame.2005.12.004.
[142] Gómez-Barea A, Ollero P, Fernández-Baco C. Diffusional Effects in CO_2 Gasification Experiments with Single Biomass Char Particles. 1. Experimental Investigation. Energy Fuels 2006;20(5):2202–10. https://doi.org/10.1021/ef050365a.
[143] Guizani C, Escudero Sanz FJ, Salvador S. Influence of temperature and particle size on the single and mixed atmosphere gasification of biomass char with H_2O and CO_2. Fuel Processing Technology 2015;134:175–88. https://doi.org/10.1016/j.fuproc.2015.01.031.
[144] Hedayati A, Sefidari H, Boman C, Skoglund N, Kienzl N, Öhman M. Ash transformation during single-pellet gasification of agricultural biomass with focus on potassium and phosphorus. Fuel Processing Technology 2021;217:106805. https://doi.org/10.1016/j.fuproc.2021.106805.

[145] Sams DA, Shadman F. Mechanism of potassium-catalyzed carbon/CO_2 reaction. AIChE J. 1986;32(7):1132–7. https://doi.org/10.1002/aic.690320710.
[146] Kopyscinski J, Rahman M, Gupta R, Mims CA, Hill JM. K2CO3 catalyzed CO2 gasification of ash-free coal. Interactions of the catalyst with carbon in N2 and CO2 atmosphere. Fuel 2014;117:1181–9. https://doi.org/10.1016/j.fuel.2013.07.030.
[147]Feng D, Zhao Y, Zhang Y, Sun S, Meng S, Guo Y et al. Effects of K and Ca on reforming of model tar compounds with pyrolysis biochars under H_2O or CO_2. Chemical Engineering Journal 2016;306:422–32. https://doi.org/10.1016/j.cej.2016.07.065.
[148] Liu Y, Yang X, Lei F, Xiao Y. Synergistic effect of alkali metals in coal and introduced CaO during steam gasification. Journal of Thermal Science 2020;29(6):1627–37. https://doi.org/10.1007/s11630-020-1250-1.
[149] Yu J, Guo Q, Gong Y, Ding L, Wang J, Yu G. A review of the effects of alkali and alkaline earth metal species on biomass gasification. Fuel Processing Technology 2021;214:106723. https://doi.org/10.1016/j.fuproc.2021.106723.
[150] Du C, Liu L, Qiu P. Importance of volatile AAEM species to char reactivity during volatile–char interactions. RSC Adv. 2017;7(17):10397–406. https://doi.org/10.1039/C6RA27485D.
[151] Ismail AF, Chandra Khulbe K, Matsuura T. Gas Separation Membranes: Polymeric and Inorganic. 1st ed. Cham: Springer; 2015.
[152]Berdugo Vilches T, Maric J, Knutsson P, Rosenfeld DC, Thunman H, Seemann M. Bed material as a catalyst for char gasification: The case of ash-coated olivine activated by K and S addition. Fuel 2018;224:85–93. https://doi.org/10.1016/j.fuel.2018.03.079.
[153]Berdugo Vilches T, Marinkovic J, Seemann M, Thunman H. Comparing active bed materials in a dual fluidized bed biomass gasifier: Olivine, bauxite, quartz-sand, and ilmenite. Energy & Fuels 2016;30(6):4848–57. https://doi.org/10.1021/acs.energyfuels.6b00327.
[154] Furusjö E, Ma C, Ji X, Carvalho L, Lundgren J, Wetterlund E. Alkali enhanced biomass gasification with in situ S capture and novel syngas cleaning. Part 1: Gasifier performance. Energy 2018;157:96–105. https://doi.org/10.1016/j.energy.2018.05.097.
[155]Wang M, Wan Y, Guo Q, Bai Y, Yu G, Liu Y et al. Brief review on petroleum coke and biomass/coal co-gasification: Syngas production, reactivity characteristics, and synergy behavior. Fuel 2021;304:121517. https://doi.org/10.1016/j.fuel.2021.121517.
[156] Wei J, Wang M, Wang F, Song X, Yu G, Liu Y et al. A review on reactivity characteristics and synergy behavior of biomass and coal Co-gasification. International Journal of Hydrogen Energy 2021;46(33):17116–32. https://doi.org/10.1016/j.ijhydene.2021.02.162.

[157]Zhang W, Huang S, Wu S, Wu Y, Gao J. Ash fusion characteristics and gasification activity during biomasses co-gasification process. Renewable Energy 2020;147:1584–94. https://doi.org/10.1016/j.renene.2019.09.058.
[158] Reinmöller M, Schreiner M, Guhl S, Neuroth M, Meyer B. Ash behavior of various fuels: The role of the intrinsic distribution of ash species. Fuel 2019;253:930–40. https://doi.org/10.1016/j.fuel.2019.05.036.
[159] Umeki K, Moilanen A, Gómez-Barea A, Konttinen J. A model of biomass char gasification describing the change in catalytic activity of ash. Chemical Engineering Journal 2012;207-208:616–24. https://doi.org/10.1016/j.cej.2012.07.025.
[160] Rebbling A, Fagerström J, Steinvall E, Carlborg M, Öhman M, Boman C. Reduction of alkali release by two fuel additives at different bed temperatures during grate combustion of woody biomass. Energy & Fuels 2019;33(11):11041–8. https://doi.org/10.1021/acs.energyfuels.9b02391.
[161]Zevenhoven-Onderwater M, Backman R, Skrifvars B-J, Hupa M. The ash chemistry in fluidised bed gasification of biomass fuels. Part I: predicting the chemistry of melting ashes and ash–bed material interaction. Fuel 2001;80(10):1489–502. https://doi.org/10.1016/S0016-2361(01)00026-6.
[162] Ren H, Zhang Y, Fang Y, Wang Y. Co-gasification behavior of meat and bone meal char and coal char. Fuel Processing Technology 2011;92(3):298–307. https://doi.org/10.1016/j.fuproc.2010.09.013.
[163] Xiang X, Gong G, Shi Y, Cai Y, Wang C. Thermodynamic modeling and analysis of a serial composite process for biomass and coal co-gasification. Renewable and Sustainable Energy Reviews 2018;82:2768–78. https://doi.org/10.1016/j.rser.2017.10.008.
[164] Huo W, Zhou Z, Chen X, Dai Z, Yu G. Study on CO_2 gasification reactivity and physical characteristics of biomass, petroleum coke and coal chars. Bioresource Technology 2014;159:143–9. https://doi.org/10.1016/j.biortech.2014.02.117.
[165] Ma Z, Bai J, Bai Z, Kong L, Guo Z, Yan J et al. Mineral transformation in char and its effect on coal char gasification reactivity at high temperatures, Part 2: Char gasification. Energy & Fuels 2014;28(3):1846–53. https://doi.org/10.1021/ef402382m.
[166] Li C-Z, Sathe C, Kershaw JR, Pang Y. Fates and roles of alkali and alkaline earth metals during the pyrolysis of a Victorian brown coal. Fuel 2000;79(3-4):427–38. https://doi.org/10.1016/S0016-2361(99)00178-7.
[167]Risnes H. Calcium addition in straw gasification. Fuel 2003;82(6):641–51. https://doi.org/10.1016/S0016-2361(02)00337-X.
[168] Lu X. Adsorption measurements in Devonian shales. Fuel 1995;74(4):599–603. https://doi.org/10.1016/0016-2361(95)98364-K.

[169] Allen SJ, McKay G, Porter JF. Adsorption isotherm models for basic dye adsorption by peat in single and binary component systems. J Colloid Interface Sci 2004;280(2):322–33. https://doi.org/10.1016/j.jcis.2004.08.078.
[170] Kapteijn F, Porre H, Moulijn JA. CO_2 gasification of activated carbon catalyzed by earth alkaline elements. AIChE J. 1986;32(4):691–5. https://doi.org/10.1002/aic.690320421.